

# The metamorphic evolution and tectonic significance of the Sumdo HP–UHP metamorphic terrane, central-south Lhasa Block, Tibet

CONG ZHANG<sup>1\*</sup>, THOMAS BADER<sup>2</sup>, HERMAN VAN ROERMUND<sup>3</sup>, JINGSUI YANG<sup>1</sup>, TINGTING SHEN<sup>1</sup>, TIAN QIU<sup>1</sup> & PENG LI<sup>1</sup>

<sup>1</sup>*Institute of Geology, Chinese Academy of Geological Sciences, Beijing, 100037, China*

<sup>2</sup>*School of Earth and Space Sciences, Peking University, Beijing, 100871, China*

<sup>3</sup>*Department of Earth Sciences, Structural Geology and Tectonics, Utrecht University, Utrecht, The Netherlands*

 C.Z., 0000-0002-0841-5476

\*Correspondence: [congzhang@pku.edu.cn](mailto:congzhang@pku.edu.cn)

**Abstract:** The Lhasa terrane, forming one of the main tectonic components of the Himalayan–Tibetan orogen, has received a lot of attention as it records multiple episodes of plate spreading, subduction and collision within the realm of the Paleo-Tethys Ocean. A review of the mineralogical, petrological, geochemical and geochronological data of eclogites, associated blueschists and garnet-bearing mica schists from the Sumdo high- and ultrahigh-pressure metamorphic (HP/UHP) complex in the central/southern part of the Lhasa terrane, is present here so that the origin and tectono-metamorphic evolution of this important suture can be deduced. By re-evaluating the original published  $P$ – $T$  conditions for the metamorphic rocks of the Sumdo Complex, we consider that the Sumdo Complex has experienced low temperature HP/UHP metamorphic conditions, characteristic of fast subduction (and exhumation) in a typical oceanic subduction zone setting. The original wide spread in the maximal peak  $P$ – $T$  conditions could be reduced in size due to thus far unknown inconsistencies in the usage of applied geothermobarometric techniques. The remaining spread in the maximal  $P$ – $T$  conditions ( $c.$  200°C/10 kbar) of the HP/UHP regions can be explained by a mechanism that the rocks from individual tectonic slices were subducted to different depths and followed by juxtaposition on their way back to the surface. A re-consideration of the isotopic ages of eclogites from the Sumdo Complex demonstrates that the opening of the Paleo-Tethys Ocean, located in between the two major components of the Lhasa terrane, was initiated prior to  $c.$  280 Ma and the eclogite facies metamorphism is likely to be of late Permian ( $c.$  260 Ma) to early Triassic age (245–225 Ma), recording different ages of subduction from individual slices of the oceanic crust. The closure of the Paleo-Tethys Ocean resulted, no earlier than 210 Ma, in the final collision between the northern and southern Lhasa blocks. This final collision event may have been triggered by the initial subduction of the Bangong–Nujiang Tethys Ocean in the north.

Since the first discovery of coesite (Chopin 1984; Smith 1984) and microdiamond (Sobolev & Shatsky 1990) within eclogite-bearing orogenic belts, extensive progress has been achieved in our understanding of the origin of ultrahigh-pressure metamorphic (UHPM) terranes formed by plate tectonic processes that involve subduction, collision, exhumation, associated mantle–lithospheric slab interactions, and geochemical recycling of subducted/exhumed rocks and fluids. Eclogites and associated (U)HP metamorphic rocks in orogenic belts record detailed pressure–temperature ( $P$ – $T$ ) information that allows a reconstruction of the pressure and temperature paths of subducted lithospheric crust with time. This, in turn, provides evidence of the thermal regime(s)

under which the various mineral assemblages equilibrated. Orogenesis involves the formation of tectonometamorphic belts that exhibit different types of regional metamorphic events that outline various tectonic settings (e.g. Chopin 2003; Ernst *et al.* 2007; Zheng 2012). Two distinct end-member types for convergent plate boundaries have been identified, the so-called Pacific- (or Andean-) and Alpine-type (or Himalayan-type) collisional margins, although a continuum of intermediate types were also identified (Liou *et al.* 2009). The Alpine-type orogen develops out of the initial consumption of an oceanic basin that separates two sialic, crust-capped, lithospheric blocks. Continuous convergence eventually results in continental subduction

From: ZHANG, L. F., ZHANG, Z., SCHERTL, H.-P. & WEI, C. (eds) 2019. *HP–UHP Metamorphism and Tectonic Evolution of Orogenic Belts*. Geological Society, London, Special Publications, **474**, 209–229.

First published online March 22, 2018, <https://doi.org/10.1144/SP474.4>

© 2018 The Author(s). Published by The Geological Society of London. All rights reserved.

For permissions: <http://www.geolsoc.org.uk/permissions>. Publishing disclaimer: [www.geolsoc.org.uk/pub\\_ethics](http://www.geolsoc.org.uk/pub_ethics)

and collision. The bedrock of this type of collisional orogen is dominated by granitic/tonalitic gneiss with minor intercalations of metapelitic, metabasic and/or ultramafic rocks of (U)HP origin, as is the case of the Western Gneiss Region in SW Norway, and the Dabie-Sulu and North Qaidam orogens in China (e.g. Carswell & Cuthbert 2003; Zhang *et al.* 2010; Song *et al.* 2014). Alternatively, the Pacific-type orogen reflects subduction of oceanic lithosphere with concomitant development of an accretionary complex, a forearc basin, a huge TTG (tonalite–trondhjemite–granodiorite) belt and/or a volcanic arc (Ernst & Liou 1995, 2008; Maruyama *et al.* 1996; Liou *et al.* 2004). The oceanic bedrock assemblage, intimately mixed with structurally dismembered ophiolites and ultramafic rocks, is commonly metamorphosed during subduction/accretion at relatively low temperatures and high/intermediate pressures: for example, the Monviso Massif in the Western Alps, and the North Qilian and western Tianshan UHP belts in western China (e.g. Chopin 1984; Philippot & van Roermund 1992; Zhang *et al.* 2003; Song *et al.* 2006).

The Lhasa terrane in SW Tibet represents one of the major core components of the Himalayan–Tibetan orogeny (Fig. 1), the Earth's youngest and probably also the most spectacular orogenic belt that formed by continent–continent collision after closure of the intermediate Tethys Ocean which was located in-between Laurasia (Qiangtang, Songpan-Ganze and Kunlun blocks, see Fig. 1b) and Gondwana (Indian Plate in Fig. 1b). The Lhasa terrane, bounded in the north by the Bangong–Nujiang Suture Zone (BNSZ in Fig. 1b) and the Indus–Yarlung Zangbo Suture Zone (YZSZ in Fig. 1b) in the south (Fig. 1b), was treated originally as a uniform terrane separated from NE Gondwana during the early Jurassic and, subsequently, accreted to Eurasia (Allegre *et al.* 1984; Yin & Harrison 2000). However, the recent identification of the Sumdo eclogites, with typical mid-ocean ridge basalt (MORB) geochemical characteristics and associated ultramafic rocks within the SE part of the Lhasa terrane, suggest that the Lhasa terrane rocks, at least in its SE part (Fig. 1b, c), were separated from each other by former inlets of the Palaeo-Tethys Ocean prior to

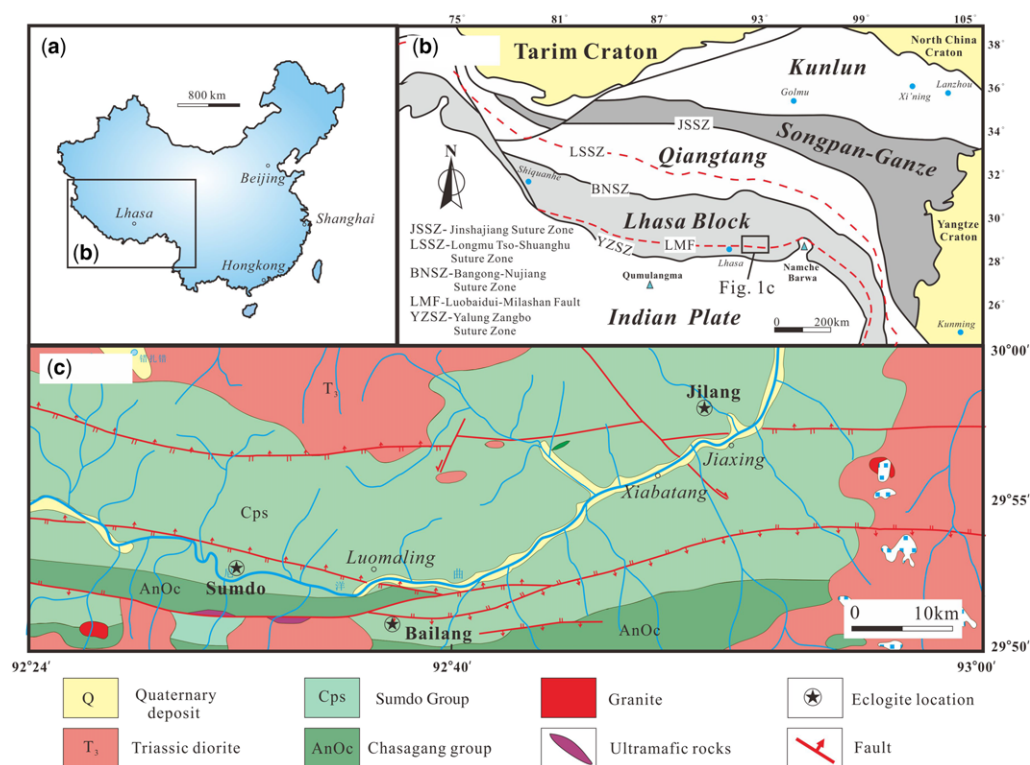


**Fig. 1.** (a) Outline map of China showing the location of the Tibetan Plateau. (b) Sketch map of the Tibetan orogen, showing the major blocks and suture zones. (c) Simplified geological map of the Sumdo area, showing the three major eclogite occurrences.

the Late Paleozoic (Yang *et al.* 2006, 2009). Further investigations of the metamorphic rocks and zircons therein showed that the entire Lhasa terrane has experienced multistage metamorphic events that include various types of regional metamorphism ranging from HP–UHP metamorphism within oceanic and/or continental subduction regimes, medium-pressure metamorphism in continent–continent collision zones to thickened crustal processes in the South Lhasa terrane between Neoproterozoic and early Cenozoic times (Zhang & Santosh 2012; Zhang *et al.* 2014 and references therein).

The (U)HP metamorphic rocks of the Sumdo Complex (called the Sumdo Group in Fig. 1c) thus form a cornerstone in the understanding of the origin, and tectonometamorphic and geochronological evolution of the leading edge of the amalgamated, southern part (or block) of the Lhasa terrane. In this way, the tectonometamorphic evolution of the Lhasa terrane can be disclosed and critical questions answered: such as when subduction of the Lhasa terranes started, when final closure of the Palaeo-Tethys Ocean took place and, last but not least, how can we use this information to place time constraints on the geodynamic evolution of the Himalayan–Tibetan orogen and/or the opening of the Tethys Ocean.

Published peak *P–T* conditions of eclogite formation in the Sumdo Complex determined using either conventional geothermobarometric methods or phase-equilibrium calculations using thermodynamic programs, such as Theriac-Domino (de Capitani & Petrakakis 2010), PerpleX (Connolly 2005) or Thermocalc (Powell & Holland 2008), range between 450 and 800°C, and between 25 and 39 kbar (e.g. Yang *et al.* 2009, 2014; Cheng *et al.* 2012, 2015). These *P–T* conditions are located within the lawsonite eclogite (LE), epidote eclogite (EE) or the dry eclogite stability fields formed by low-temperature (LT)–medium-temperature (MT) metamorphism. However, models explaining this large spread in *P–T* conditions inside a single subduction zone complex are lacking. In addition, published zircon U–Pb and garnet Lu–Hf and Sm–Nd isotopic ages of eclogites from the Sumdo, Jilang and Bailang areas, which together define the Sumdo Complex, spread over more than 100 myr from 304 Ma (Carboniferous) to c. 200 Ma (late Triassic) (e.g. Yang *et al.* 2009; Cheng *et al.* 2012, 2015) and provide poor constraints on the metamorphic evolution of this (U)HP orogenic belt (Fig. 1). In this contribution, we will therefore critically review the representative mineralogical, petrological, geochemical and geochronological data of eclogites, and related blueschist and garnet-bearing mica schists from the Sumdo Complex in order to: (1) constrain in much greater detail the timing of the metamorphic evolution; (2) unravel the tectonic significance of the Sumdo (U) HP metamorphic belt; and (3) reconstruct the

geodynamic settings of the Palaeo-Tethys Ocean and the formation of the Lhasa terrane.

## Geological setting

The Himalayan–Tibetan orogenic belt is classically considered to be composed of four continental blocks/terrane that are called, from north to south, the Songpan–Ganzi, Qiangtang, Lhasa and Tethyan–Himalayan (or Indian Plate in Fig. 1b) terranes. These four terranes are separated by the Jinsha Suture Zone (JSSZ), the Bangong–Nujiang Suture Zone (BNSZ) and the Yarlung Zangbo Suture Zone (YZSZ), interpreted to represent major structural elements of the Paleo-, Meso- and Neo-Tethys oceanic domains, respectively (e.g. Yin & Harrison 2000; Shi *et al.* 2008; Gehrels *et al.* 2011). These three major suture boundaries were formed after progressive rifting events along the NE margin of Gondwana, followed by northwards drift of the various terranes until they collided first with the SE Asian margin (Tarim and Kunlun blocks in Fig. 1b) or, later in time, with one of the accreted blocks (Songpan–Ganze; Qiangtang and/or Lhasa). The Paleo-, Meso- and Neo-Tethys oceanic domains were created and consumed between these distinct continental terranes, rather than indicating separate and unconnected oceans (Guynn *et al.* 2012). However, more recent investigations have revealed that this so-called Himalayan–Tibetan orogenic belt contains more complex components and, consequently, its evolutionary history is far more complex than previously anticipated (Li *et al.* 2006; Pullen *et al.* 2008; Zhai *et al.* 2011). These recent investigations include the identification of a major Triassic plate boundary characterized by an ophiolite unit and an associated HP metamorphic belt, termed the Longmu Tso–Shuanghu Suture Zone (LSSZ in Fig. 1b), extending in a NW–SE direction across the entire Qiangtang terrane and, as such, dissecting it into the South and North Qiangtang terranes (e.g. Li *et al.* 2006; Pullen *et al.* 2008; Zhai *et al.* 2011).

The Lhasa terrane, discussed in this paper, is located in the southern part of Tibet where it forms a large crustal segment with a width of 100–300 km and a length of c. 2000 km (Fig. 1). It was speculated as having rifted from Gondwana in the Triassic or the Middle–Late Jurassic and drifted northwards across the Tethyan Ocean before it collided with the Qiangtang Block of the Eurasian continent to form the BNSZ (Fig. 1b) in the Cretaceous. This interpretation is based on the widespread occurrence of Carboniferous–Permian diamictites, and Gondwana flora and fauna (Leeder *et al.* 1988; Metcalfe 1996). Another palaeogeographical interpretation suggests that the Lhasa terrane was located alongside NW Australia (forming part of Gondwana)

in the late Carboniferous. The latter interpretation assumes southwards subduction of the eastern Palaeo-Tethys, and reinterprets the Permian volcanic rocks of the northern Lhasa terrane as arc-related rather than rift-related rocks (Ferrari *et al.* 2008; Zhu *et al.* 2011a). An Andean-type active continental margin, composed of the Xigaze forearc basin sequence in the north and the Gangdese batholith in the south, has also been proposed for the southern part of the Lhasa terrane prior to its collision with the northwards-moving Indian Plate in the Cenozoic. The latter is marked by the YZSZ (in Fig. 1b) (e.g. Sengör 1984; Yin & Harrison 2000; Kapp *et al.* 2007; Zhu *et al.* 2011b).

The Lhasa terrane is composed dominantly of the underlying crystalline basement of Precambrian age, Palaeozoic–Mesozoic marine strata, and Mesozoic and Cenozoic arc-type volcanic rocks and intrusions (e.g. Yin & Harrison 2000; Zhu *et al.* 2009, 2011b, 2013; Pan *et al.* 2012; Zhang & Santosh 2012). This trifold tectonostratigraphy was used to divide the entire Lhasa terrane into three belts called the northern, central and southern sub-terrane, separated by the Shiquan River–Nam Tso Fault and the Luobadui–Milashan Fault, respectively. The southern Lhasa sub-terrane is dominated by the Cretaceous–Tertiary Gangdese batholiths and the Paleogene Linzizong volcanic succession, with minor Triassic–Cretaceous volcanosedimentary rocks, indicating a juvenile crust with its underlying Precambrian crystalline basement only locally preserved (e.g. Mo *et al.* 2008; Zhu *et al.* 2012). The central Lhasa sub-terrane represents a microcontinent with Precambrian crystalline basement rocks, covered by Cambrian–Permian meta-sediments and Upper Jurassic–Lower Cretaceous sedimentary units with abundant volcanic rocks, as well as minor Ordovician, Silurian, Devonian and Triassic limestone (Zhu *et al.* 2011a; Pan *et al.* 2012). The northern Lhasa sub-terrane has traditionally been interpreted to be underlain by a Cambrian or Neoproterozoic crystalline basement, as exemplified by the orthogneisses of Amdo (Gynn *et al.* 2006). However, recent studies have shown that the Amdo microcontinent is not an integral part of the northern Lhasa sub-terrane, but consists of juvenile crust covered by Middle Triassic–Cretaceous sedimentary rocks with abundant early Cretaceous volcanic rocks and associated granitoids (Zhu *et al.* 2011b, 2012; Z.M. Zhang *et al.* 2012).

Based on the recognition of eclogite in Sumdo and blueschist in Pana, c. 80 km west of Sumdo, a new subdivision of the Lhasa terrane has been proposed (Liu *et al.* 2009; Yang *et al.* 2009). These authors suggested that the Lhasa terrane consists of two discrete crustal fragments, the South and North Lhasa terranes, the latter of which includes the former central and northern Lhasa sub-terrane as described above. Zhu *et al.* (2013) proposed that

the two terranes are separated by the Luobadui–Milashan Fault, which represented a Carboniferous–Permian suture zone forming the boundary between the North and South Lhasa terranes. The latter interpretation is based on the following three arguments: (1) the Sumdo eclogite exhibits typical MORB geochemical signatures, and probably represents remnants of the upper parts of the former Palaeo-Tethyan oceanic lithosphere; (2) the ultramafic peridotite in the Sumdo eclogitic belt, which probably represents remnants of basal sections of the Palaeo-Tethyan oceanic lithosphere; and (3) zircon Hf-isotope data from magmatic rocks support a westwards extension of the Carboniferous–Permian suture zone. According to this new model of Zhu *et al.* (2013), the southern Palaeo-Tethys Ocean subducted northwards below the southern margin of the South Lhasa terrane, leading to a collision between the South Lhasa terrane and NW Australia during the Late Permian.

The Sumdo eclogite-bearing complex (or group; see Fig. 1c) forms in an east–west-trending belt at least 100 km long and up to 10 km wide, located about 180 km east of Lhasa city (Fig. 1b). It consists dominantly of metamorphosed quartzite and pelitic schist, with minor marble, metabasic lenses and serpentized ultramafic bodies. The eclogite lenses are hosted by the meta-sedimentary strata. Fresh eclogitic garnet–omphacite mineral assemblages are preserved only in some of the cores of the metabasic boudins, which otherwise contain amphibole (retro-) eclogite, garnet amphibolite or amphibolite-facies mineral assemblages especially in boudin rims (Fig. 2). Within the Sumdo eclogites-bearing belt (Fig. 1c), eclogites have been reported and studied from three major locations, from west to east, called Sumdo, Bailang and Jilang, located c. 50 km apart (Fig. 1c). The Sumdo eclogite was discovered first in 2006 and has been particularly studied since then (Yang *et al.* 2006, 2009, 2014; Chen *et al.* 2009, 2015; H.Q. Li *et al.* 2009; Zeng *et al.* 2009; Zhang *et al.* 2011; Huang *et al.* 2015; Weller *et al.* 2016). In addition, Cheng *et al.* (2012, 2015) have carried out detailed mineralogical, petrological and geochronological investigations of the Jilang and Bailang eclogites, respectively.

## Calculated metamorphic conditions for UHP rocks from the Sumdo Complex

### Sumdo area

The Sumdo HP–UHP metamorphic belt has been discovered near the village of Sumdo. Subsequent mineralogical, petrological and microchemical investigations clearly demonstrated that at least some of these rocks were metamorphosed under





**Fig. 2.** Field occurrence of the eclogite and its country rock schist. (a) Phengite-bearing eclogite from the Sumdo area. (b) Garnet-bearing mica schist constituting the country rock of eclogite. (c) Retrograde eclogite within mica schist occurring in the Bailang area. (d) Fine-grained fresh eclogite from the Jilang area.

UHPM conditions (Yang *et al.* 2006) (Fig. 1c). Since then, various research groups have studied many different eclogite bodies from the Sumdo area, examples of which are rutile eclogite, quartz eclogite, phengite eclogite and glaucophane eclogite (Yang *et al.* 2009; Huang *et al.* 2015; Weller *et al.* 2016). In the following subsection, despite the difference in diagnostic minerals, we have treated rutile, quartz and phengite eclogite as the same type of phengite eclogite. Accordingly, we have treated these rocks below as a single rock type called glaucophane eclogite.

**Phengite eclogite.** Fresh phengite eclogite preserved in cores of larger boudins is greyish-green in colour and ‘massive’ (although a weak eclogitic foliation can sometimes be seen, defined by the shape-preferred orientation of omphacite crystals). Phengite eclogites are composed of garnet (50–60%), phengite (10–20%), omphacite (10–20%), amphibole (10%), zoisite (5%) and minor rutile (Fig. 3a). Garnet is commonly fractured and occurs as euhedral to anhedral porphyroblasts, approximately 0.5–3 mm in diameter, that often contain inclusion-rich cores containing calcic amphibole, apatite, chlorite, quartz, rutile and titanite. In contrast, garnet rims contain minor amounts of phengite, quartz or rutile.

Electron microprobe (EMP) chemical line scans across garnet grains are moderately variable, but consistent core–rim garnet patterns were measured in all cases where Mn was observed to decrease from core to rim. The latter pattern is defined by garnet core regions that have high contents of Mn and Ca, while both elements decrease rimwards alongside increasing Mg and Fe contents. This chemical zoning pattern in garnet is interpreted to reflect prograde metamorphic growth. Inclusion-poor rims of garnet grains are notable for having sharply increasing Mg, compared to the relatively flat Ca contents. Omphacite forms anhedral porphyroblasts, with increasing jadeite contents of 25 mol% in grain cores to 50 mol% in rims. Amphibole is present as light-green actinolite crystals that are surrounded by dark-green pargasitic rims interpreted as replacement products of the peak garnet + omphacite assemblage during retrograde metamorphism. Matrix phengite exhibits a core to rim decrease in Si from 3.6 to 3.2 pfu. As the phengite content of white mica typically increases with pressure, this reverse zonation suggests that re-equilibration occurred during decompression, with the highest phengite content being representative of peak metamorphic conditions. Epidote porphyroblasts are observed in the matrix of amphibole-rich regions and interpreted



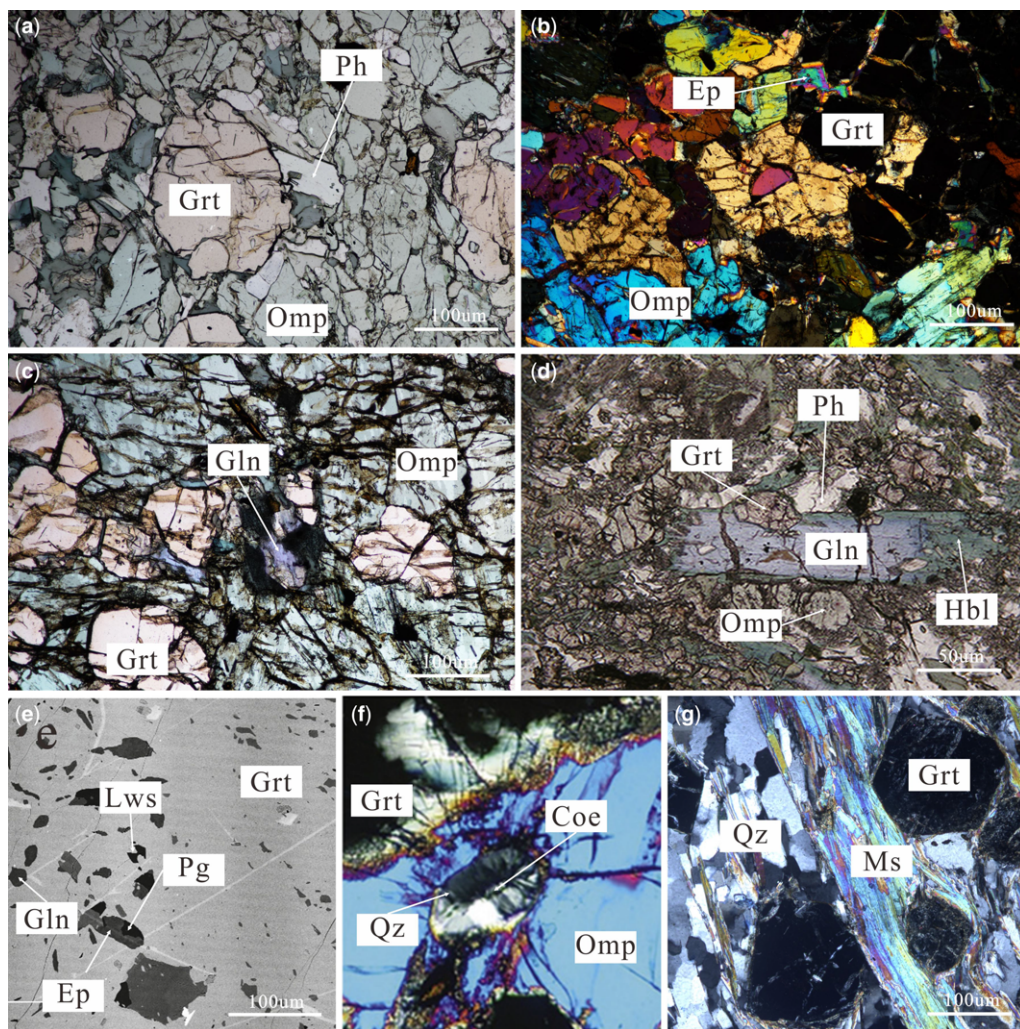


**Fig. 3.** Photomicrographs and backscattered-electron images of eclogite and garnet-bearing mica schist from the Sumdo, Jilang and Bailang areas. (a) Photomicrograph of phengite eclogite from the Sumdo area under plane-polarized light. (b) Phengite eclogite from the Jilang area under cross-polarized light. (c) Photomicrograph of glaucophane eclogite from the Sumdo area, plane-polarized light. (d) Glaucophane eclogite from the Bailang area showing glaucophane with a hornblende rim, from [Cheng \*et al.\* \(2015\)](#). (e) Backscattered-electron image showing a lawsonite inclusion in garnet from the Bailang eclogite, from [Cheng \*et al.\* \(2015\)](#). (f) Cross-polarized light image showing a coesite inclusion in omphacite from Jilang eclogite, from [Cheng \*et al.\* \(2012\)](#). (g) Photomicrograph of a garnet-bearing mica schist from the Sumdo area, which is the country rock of the eclogite.

as a retrograde segment. Quartz rods, present as exsolution lamella in omphacite, and a number of quartz inclusions inside omphacite and garnet have radially arranged expansion fractures around them, indicating that the  $\text{SiO}_2$  inclusions may be pseudomorphs after coesite. The latter microstructure was used as microstructural evidence that the phengite eclogite was formed under UHPM conditions ([Yang \*et al.\* 2009](#)). However, *in situ* coesite crystals

have not been found so far in the phengite eclogites of the Sumdo area.

By using the garnet–clinopyroxene  $\text{Fe}^{2+}$ –Mg exchange geothermometer of [Krogh Ravna \(2000\)](#) in combination with the garnet–omphacite–phengite geobarometer (GCP: [Krogh Ravna & Terry 2004](#)), MT UHP metamorphic conditions were calculated: that is, 730°C at c. 27 kbar and 760–780°C at 33–39 kbar (Fig. 4) ([Yang \*et al.\* 2009](#); [Zhang \*et al.\*](#)

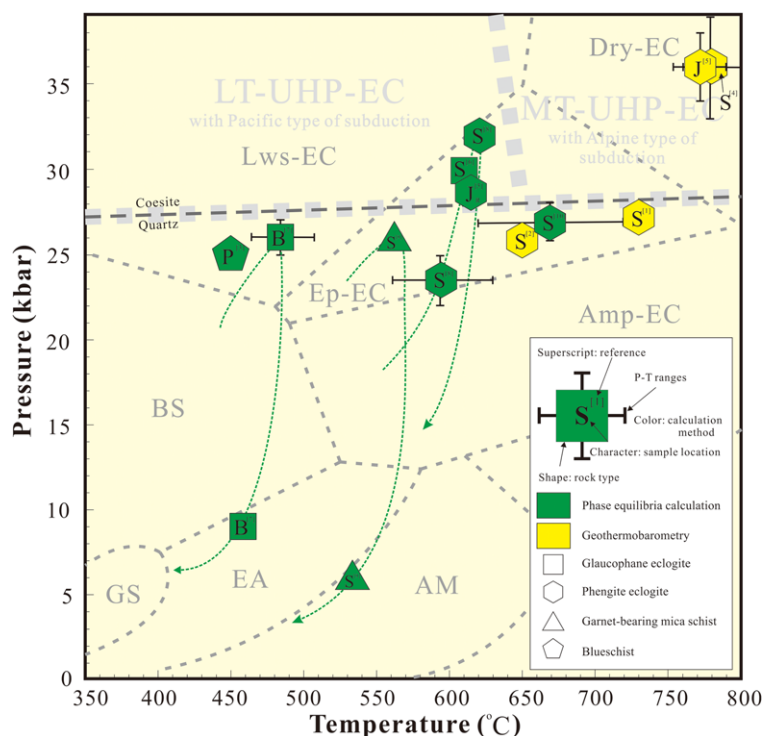


**Fig. 4.** Schematic  $P$ – $T$  conditions comparison for metamorphic processes of eclogites and schist from the Lhasa terrane. The  $P$ – $T$  boundaries of various metamorphic facies are indicated: AM, amphibolite; EA, epidote amphibolite; GS, greenschist; BS, blueschist schist. The subdivisions of eclogite (EC) of amphibole eclogite (Amp-EC), epidote eclogite (Ep-EC), lawsonite eclogite (Lws-EC) and dry eclogite are also indicated. The division between low-temperature ultrahigh-pressure eclogite (LT-UHP-EC) and medium-temperature ultrahigh-pressure eclogite (MT-UHP-EC) is taken from (Wei *et al.* 2013). The letter inside the  $P$ – $T$  symbols gives the sample location: S, sumdo; J, Jilang; JR, Jilang recalculated condition; B, Bailang; P, Pana. Indicated references are: [1] Yang *et al.* (2009); [2] Zeng *et al.* (2009); [3] Liu *et al.* (2009); [4] Zhang *et al.* (2011); [5] Cheng *et al.* (2012); [6] Yang *et al.* (2014); [7] Cheng *et al.* (2015); [8] Huang *et al.* (2015); [9] Chen *et al.* (2015); [10] Weller *et al.* (2016).

2011). More recently, lower temperatures, but still HP–UHP metamorphic conditions (620–670°C at 27–32 kbar), were documented using phase-equilibrium calculations by Thermocalc (Huang *et al.* 2015; Weller *et al.* 2016). All these calculated  $P$ – $T$  conditions are interpreted here to be representative of the peak metamorphic conditions for phengite eclogite formation in the Sumdo area.

**Glaucophane eclogite.** Glaucophane eclogite in Sumdo is composed of garnet (25–30%), omphacite (30–35%), glaucophane (10–15%), epidote/clinozoisite (10–15%), and minor rutile, phengite, hornblende and quartz (Fig. 3c). Garnet porphyroblasts show compositional zoning in which the pyrope (MgAl) component increases and grossular (CaAl) decreases from core to rim. In addition, the outer rims of garnets contain a grossular-rich rim interpreted to be due to retrogression. Glaucophane is found as secondary grains in the matrix or as primary

inclusions in garnet. In the latter case, it is commonly rimmed by barrosite, which indicates that these inclusions in garnet are not only formed during the prograde metamorphic stages. Most omphacite crystals reveal a weak compositional zoning. The ones which grow in equilibrium with prograde garnet show an increase in jadeite content from core to rim; those associated with secondary glaucophanes have an opposite chemical trend that is defined by an aegirite ( $\text{NaFe}^{3+}$ ) component that increases towards the rim. Glaucophane and omphacite are commonly transformed into plagioclase–amphibole symplectites. Garnet is usually rimmed by coronas of pargasitic amphibole. Phengite crystals included in garnet have higher Si (3.61 pfu) contents than the ones in the matrix (Si = 3.46 pfu). The  $P$ – $T$  conditions of glaucophane eclogite were calculated using pseudosections in the model system of NCKMnFMASHTO and with the aid of the thermodynamic program Thermocalc (Yang *et al.* 2014).

The  $P$ – $T$  results indicate peak metamorphic conditions of  $30 \pm 0.6$  kbar and  $610 \pm 6^\circ\text{C}$ , using the intersection point(s) between the isopleths of the maximum pyrope content in garnet and the maximum Si content in phengite (Fig. 4). The moderate slope ( $c. 7\text{--}8^\circ\text{C km}^{-1}$ ) of the prograde  $P$ – $T$  path, calculated using core and rim garnet compositions, indicates that the rock has experienced heating while pressure increased less. These calculations are consistent with the early stages of a slow subduction process. However, calculations using the garnet compositions of the ‘grossular-rich’ mantle and a ‘normal’ garnet rim composition, in combination with the Si content of phengite, resulted in an opposite slope in  $P$ – $T$  space characterized by slow heating and a relatively fast increase in pressure, which means it went into a fast subduction stage in which the geotherm decreased to  $c. 5\text{--}6^\circ\text{C km}^{-1}$ . After the peak metamorphic stage, glaucophane eclogite experienced an early retrograde stage of isothermal decompression, followed by a later stage of retrogression characterized by the complete transformation of lawsonite into secondary glaucophane and epidote; while barrosite formed around primary glaucophane was interpreted to be due to an Fe-enrichment event related to the income of fluids. The isothermal decompression period, recorded by glaucophane eclogites, probably reflects a fast tectonic exhumation process (Yang *et al.* 2014).

**Garnet-bearing mica schist.** The garnet-bearing mica schist of Sumdo is mainly composed of garnet, white mica, albite and quartz. Chlorite, rutile and sphene are present as accessory minerals (Figs 2b & 3g). In EMP line scans, garnet reveals prograde chemical-zoning patterns in core–rim/mantle profiles in which the pyrope content is increasing and the spessartine contents are decreasing, including the distinct modified garnet mantle composition, interpreted to have formed during decompression (Chen *et al.* 2015). The model system of NCKMnFMASHO was used to calculate pseudosections in Thermocalc; and by applying the intersection method between various garnet isopleths, the maximum  $P$ – $T$  conditions of the garnet-bearing mica schist were calculated. Results are presented in Figure 4 and Table 1. The modelling suggests that the garnet-bearing mica schist was metamorphosed at eclogite-facies  $P$ – $T$  conditions of  $c. 27$  kbar and  $c. 580^\circ\text{C}$ . The compositional core–rim/mantle profiles in garnet imply that the prograde blueschist-to eclogite-facies metamorphism proceeded during cold subduction, with heating and compression during a fast exhumation process (Chen *et al.* 2015).

**Blueschist in Pana.** Blueschist was recognized in the Pana area,  $c. 80$  km west of the Sumdo area. It consists of  $c. 10\%$  corroded garnet porphyroclasts

and larger grains of glaucophane that are floating in a finer-grained matrix of white mica, epidote, chlorite, biotite, albite, quartz and accessory rutile, titanite, and apatite. The larger glaucophane crystals are surrounded by fine-grained barrosite and Ca-amphibole. The garnet grains are  $c. 1$  mm in diameter with spessartine contents decreasing from core to rim, showing a weak prograde zonation. Aegirine-rich clinopyroxene is found as inclusions in garnet. No omphacite occurrences were documented in the previously mentioned literature. Amphibole changes in composition from glaucophane through Na–Ca-amphibole to Ca-amphibole. The Si contents of phengite are high in the core (3.51 pfu) and low in the rim (3.25 pfu). Phase-equilibrium calculations using PerpleX show that the  $P$ – $T$  path starts around 25 kbar,  $450^\circ\text{C}$ . An increase in temperature up to  $500^\circ\text{C}$  can then be documented followed by isothermal decompression through the blueschist facies down to 6 kbar (Fig. 4). This calculated  $P$ – $T$  path may indicate that the rock originated from a cold subduction environment (Liu *et al.* 2009).

### *Jilang phengite eclogite*

The phengite eclogite in Jilang is present as a lens-like body ( $c. 30$  m in diameter) inside quartzite (Figs 1c & 2d). The lens is coarse grained, and consists mainly of garnet, omphacite, amphibole and phengite, with minor amounts of zoisite, rutile and quartz (Fig. 3b). Garnets, ranging from 0.5 to 1.0 mm in size, have mostly hypidioblastic–idioblastic shapes, and are loaded with inclusions of phengite, rutile, quartz/coesite and omphacite. Zoisite and amphibole are mostly retrograde metamorphic phases replacing omphacite. Coesite inclusions have been identified inside omphacite crystals from the Jilang eclogite (Cheng *et al.* 2012). These  $\text{SiO}_2$  inclusions are surrounded by outwards-radiating fractures that typically extend to the edge of the host omphacite. The  $\text{SiO}_2$  inclusion itself consists of a core of high-relief coesite that is surrounded by a fine-grained polycrystalline rim of quartz (Fig. 3f).

Garnet porphyroblasts have inclusion-free rims and an inclusion-rich core with abundant inclusions of phengite, omphacite and quartz, and a Mn-poor, inclusion-free, outer rim. The zoning profiles shows an increase in Mg and a decrease in Mn from core to rim. Omphacite occurs as blocky crystals (typically  $c. 1.0$  mm) in the matrix and are randomly orientated. Omphacite grew in textural equilibrium with garnet and has jadeite components of 21–51 mol%. Omphacite inclusions in cores of garnet are less sodic than adjacent omphacite crystals in the matrix, whereas omphacite inclusions in garnet rims resemble omphacite core compositions in the matrix. Matrix omphacite is chemically zoned,



**Table 1.** Summarized calculated P–T conditions and ages of the HP–UHP rocks in the Sumdo (U)HP metamorphic belt, Tibet

Location	Rock type	P–T conditions				Geochronology			Reference
		P (kbar)	T (°C)	Technique	Stage	Age	Technique	Interpretation	
Sumdo	Phengite eclogite	c. 27	730	Geothermobarometry	Peak	262 ± 5	Zircon U–Pb SHRIMP	Eclogite-facies metamorphism	Yang <i>et al.</i> (2009)
	Phengite eclogite	26	650	Geothermobarometry	Peak	239 ± 3.5	Garnet–omphacite–whole rock Sm–Nd	Eclogite-facies metamorphism	Zeng <i>et al.</i> (2009)
	Schist					220–230	Muscovite <sup>40</sup> Ar/ <sup>39</sup> Ar	Greenschist- to amphibolite-facies metamorphism	H.Q Li <i>et al.</i> (2009)
	Schist					230 ± 2–241 ± 3	Muscovite <sup>40</sup> Ar/ <sup>39</sup> Ar		Li <i>et al.</i> (2011)
	Eclogite					224 ± 2–234 ± 3	Muscovite <sup>40</sup> Ar/ <sup>39</sup> Ar		
						235 ± 3	Amphibole <sup>40</sup> Ar/ <sup>39</sup> Ar		
	Phengite eclogite	33–39	760–800	Geothermobarometry	Peak				Zhang <i>et al.</i> (2011)
	Glaucophane eclogite	30 ± 0.6	610 ± 6	Thermocalc	Peak		Muscovite <sup>40</sup> Ar/ <sup>39</sup> Ar		Yang <i>et al.</i> (2014)
	Phengite eclogite	32	620	Thermocalc	Peak				Huang <i>et al.</i> (2015)
Pana	Garnet-bearing mica schist	27	580	Thermocalc	Near peak				Chen <i>et al.</i> (2015)
	Phengite eclogite	27 ± 1	670 ± 50	Thermocalc	Peak	274 ± 3	Zircon U–Pb SHRIMP	Protolith zircon recrystallization	Weller <i>et al.</i> (2016)
Jilang	Blueschist	25–27	450–500	Perple_X	Prograde to peak				Liu <i>et al.</i> (2009)
Jilang	Phengite eclogite	34–38	753–790	Geothermobarometry	Peak	265.9 ± 1.1	Garnet–omphacite–whole rock Lu–Hf	Eclogite-facies metamorphism	Cheng <i>et al.</i> (2012)
						261.2 ± 3.1	Zircon U–Pb LA-ICP-MS	Eclogite-facies metamorphism	
						238.1 ± 3.2	Zircon U–Pb LA-ICP-MS	Retrograde metamorphism	
						290.6 ± 6.2	Zircon U–Pb LA-ICP-MS	Protolith	
						291 ± 4	Zircon U–Pb LA-ICP-MS		
	Quartzite								
	Eclogite					230 ± 2	Muscovite <sup>40</sup> Ar/ <sup>39</sup> Ar		Li <i>et al.</i> (2011)
	Glaucophane eclogite	25–27	465–503	Geothermobarometry	Peak	238.1 ± 3.6	Garnet–omphacite–whole rock Lu–Hf	Pre-eclogite facies	Cheng <i>et al.</i> (2015)
						230.0 ± 4.7	Garnet–omphacite–whole rock Sm–Nd	Eclogite-facies metamorphism	
						227.4 ± 6.4	Zircon U–Pb SIMS	Eclogite-facies metamorphism	
Bailang	Glaucophane eclogite					304 ± 5	Zircon U–Pb SIMS	Protolith	
						200	Amphibole <sup>40</sup> Ar/ <sup>39</sup> Ar	Exhumation age	

with increasing jadeite contents toward the rim. Phengite is usually observed as large flakes, generally *c.* 0.5 mm in size. The Si content in the cores (Si = 3.6 pfu) of matrix phengites is generally higher than that in the rims (Si = 3.5 pfu). Minor retrograde textures that are present involve the breakdown of omphacite into Na–Ca-amphibole-rich and plagioclase symplectites.

Two approaches were used to calculate *P–T* conditions for Jilang eclogites: (1) geothermobarometry and (2) phase-equilibrium calculations. Conventional garnet–clinopyroxene Fe<sup>2+</sup>–Mg geothermometry (Krogh Ravna 2000) was used in combination with garnet–omphacite–phengite geobarometry (Krogh Ravna & Terry 2004), and was applied to mineral compositions that have the highest pyrope content in garnet, the highest jadeite content in omphacite and the highest Si content in phengite. The calculated *P–T* conditions are 34–38 kbar and 753–790°C (Fig. 4), which suggests MT and UHPM conditions (Table 1), and are also consistent with the findings of the UHP SiO<sub>2</sub> polymorph coesite inside omphacite (Cheng *et al.* 2012). Alternatively, using the thermodynamic software Theriak-Domino with a modal system of NCKFMASH yielded *P–T* conditions of 29 kbar and 610°C (Fig. 4), which correspond to LT and UHP metamorphic conditions, and were calculated using the intersection method between the isopleths of highest X<sub>Prp</sub> content (0.30) in garnet and highest Si content (3.6 pfu) in phengite. The latter calculated *P–T* conditions are, however, 140–180°C lower than the results calculated by the geothermobarometric method (Fig. 4).

### *Bailang glaucophane eclogite*

Bailang is located *c.* 20 km east of Sumdo. The eclogite samples were collected from variably sized (1–20 m in diameter) eclogite bodies surrounded by quartz–mica schists (Figs 1c & 2c). The Bailang eclogite samples consist of mineral assemblages defined by idiomorphic garnet (*c.* 45 vol%), set in a matrix of omphacite (*c.* 30 vol%), amphibole (10–20 vol%), epidote (*c.* 5 vol%) and phengite (*c.* 5 vol%), with accessory amounts of rutile, quartz, paragonite and chlorite. Only small amounts of glaucophane are present in eclogite, most of them are retrogressed to hornblende (Fig. 3d). Lawsonite is observed only as inclusions in garnet (Fig. 3e). *In situ* coesite and/or typical quartz pseudomorphic microstructures after coesite have not been found. Porphyroblastic garnets form characteristic microstructures with grain cores crowded with tiny mineral inclusions and (outer) garnet rims that reveal much fewer mineral inclusions. All garnet porphyroblasts contain similar inclusion assemblages: epidote, omphacite, rutile, quartz, glaucophane, lawsonite, chlorite and box-shaped microdomains containing

aggregates of epidote + paragonite ± phengite, which might represent pseudomorphs after lawsonite. Garnet is almandine-rich and exhibits chemical-zoning patterns that are characteristic of the prograde growth of garnet, exemplified from core to rim by increasing pyrope and grossular contents, and decreasing almandine and spessartine contents. Clinopyroxene is found as small subhedral–anhedral grains in the matrix, or as inclusions inside garnet or epidote porphyroblasts. Clinopyroxene is practically unzoned and contains 41–47 mol% jadeite. Phengite has Si contents between 3.3 and 3.6 pfu, and occurs commonly as fine-grained, subhedral flakes in the matrix where it defines a weak foliation together with glaucophane and omphacite. Paragonite occurs together with epidote and/or phengite in the earlier described box-shaped aggregates included in garnet (Fig. 3e). Glaucophane appears as small matrix grains or as inclusions in garnet; a few larger glaucophane porphyroblasts are also observed overgrowing the matrix foliation. Epidote occurs as inclusions in garnet or as porphyroblasts in the matrix. The latter may contain inclusions of garnet, glaucophane and rutile (Cheng *et al.* 2015).

### Geochemical characteristics of eclogite

Major element, trace element and Sr–Nd isotope analysis were performed on eclogites from Sumdo, Jilang and Bailang areas in order to reconstruct the tectonic environment of the eclogitic protoliths. With 43–50% SiO<sub>2</sub> content, high CaO and relatively low K<sub>2</sub>O content, the eclogite from the Sumdo area plots in the tholeiite field of the AFM diagram, indicating that the eclogitic protolith was derived from a low potassium tholeiitic basalt or gabbro (Z.L. Li *et al.* 2009; Yang *et al.* 2009). Strongly depleted light rare earth element (LREE) and flat heavy rare earth element (HREE) distribution patterns with weak or no negative Eu anomalies show that the eclogite has similar geochemical characteristics to typical normal mid-ocean ridge basalt (N-MORB) (Fig. 5) (Zeng *et al.* 2009). The latter interpretation is also in agreement with results from the V–Ti discrimination diagram of Yang *et al.* (2009). Z.L. Li *et al.* (2009) have plotted their measured Sr–Nd isotopic data in the <sup>87</sup>Sr/<sup>86</sup>Sr v. <sup>143</sup>Nd/<sup>144</sup>Nd diagram, and compared the eclogite in the Sumdo area with typical continental-derived eclogite. Sumdo eclogites are characterized by a low Rb/Sr ratio and a high Sm/Nd ratio, which is obviously different to Dabieshan eclogite. The uniform high positive ε<sub>Nd(0)</sub> value (*c.* +8) is similar to eclogite in the Armorican Complex of France and the Cabo Ortegal Complex of Spain, which is believed to have formed by subduction of oceanic lithosphere (Bernard-Griffiths & Cornichet 1985). On the basis of the

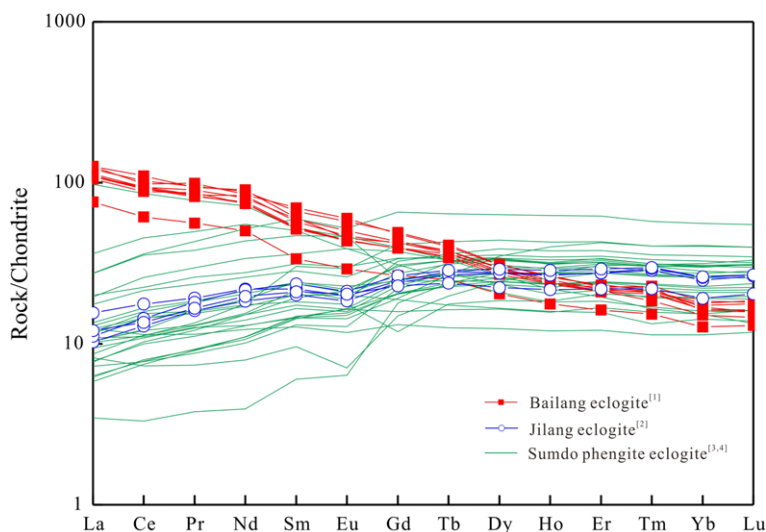


**Fig. 5.** The rare earth element (REE) distribution pattern of the eclogites in the Sumdo Complex. Indicated references are: [1] Cheng *et al.* (2015); [2] Cheng *et al.* (2012); [3] Zeng *et al.* (2009); [4] Z.L. Li *et al.* (2009).

geochemical and isotopic characteristics described above, the Sumdo eclogite is interpreted to be of N-MORB affinity.

Eclogite from the Jilang area shows similar N-MORB geochemical characteristics to the Sumdo eclogite (Fig. 5). They are, however, also characterized by low contents of incompatible elements (Zr, Nb and Th) that are normally enriched in continental crust. In addition, their low Th/Yb ratios are more comparable to intra-oceanic supra-subduction zone basalts (either from island arc or back-arc settings) than to tholeiitic continental basalts. The high Zr/Nb ratios, low Nb concentrations and negative Nb–Ta anomalies appear to disprove an ocean island basalt (OIB) type (Spandler *et al.* 2004). Based on the evidence of clearly negative Nb anomalies in the MORB-normalized spider diagram and the positive Pb anomaly (Cheng *et al.* 2012), it can be proposed that the protolith of Jilang eclogite is more likely to resemble that of a back-arc basin basalt (BABB) formed in a supra-subduction-zone setting.

Eclogite samples from the Bailang area have similar major element compositions that resemble basaltic bulk rock composition. The rocks have high TiO<sub>2</sub> (3.05–3.83 wt%) contents and relatively low MgO (4.84–6.01 wt%), which suggest a slightly alkaline tholeiitic composition (Cheng *et al.* 2015). Chondrite-normalized REE distribution patterns show a LREE-enriched pattern without a Eu anomaly (Fig. 5). The Bailang eclogites have MORB-normalized trace-element patterns showing enrichment in Rb and Ba, marked negative Sr anomalies, and no significant depletion in Ta, Nb, Zr and Hf,

resembling the patterns for enriched basalts of near-ridge seamounts or OIBs. An OIB affinity for the Bailang eclogites is also suggested using discrimination diagrams, such as Ti v. V, FeO/MgO v. TiO<sub>2</sub> and Al<sub>2</sub>O<sub>3</sub> v. TiO<sub>2</sub> diagrams (Cheng *et al.* 2015).

## Geochronology

### *Sumdo eclogites*

To constrain the timing of the different evolutionary stages, zircons from the Sumdo phengite eclogite were dated using the sensitive high-resolution ion microprobe (SHRIMP) and laser ablation-inductively coupled plasma-mass spectrometry (LA-ICP-MS) techniques (Chen *et al.* 2009; Yang *et al.* 2009). In addition, Sm–Nd and Ar/Ar isotopic investigations (Z.L. Li *et al.* 2009, 2011; Zeng *et al.* 2009) were performed on Sumdo phengite eclogite. However, so far, no geochronological age data from the glaucophane eclogite has been reported.

Individual zircon grains may contain evenly distributed mineral inclusions of garnet, omphacite, quartz and/or rutile. Zircon SHRIMP ages for phengite eclogite range between  $293 \pm 13$  and  $242 \pm 15$  Ma, with an average value of  $262 \pm 5$  Ma (MSWD = 1.08) (Fig. 6; Table 1), suggesting that the zircons crystallized during the eclogite-facies metamorphism. The latter interpretation is also supported by a uniform microtexture of the zircons in cathodoluminescence (CL) images (Yang *et al.* 2009). Weller *et al.* (2016) published recently *in situ* SHRIMP zircon ages collected in phengite eclogite from the same outcrop. Their results yielded



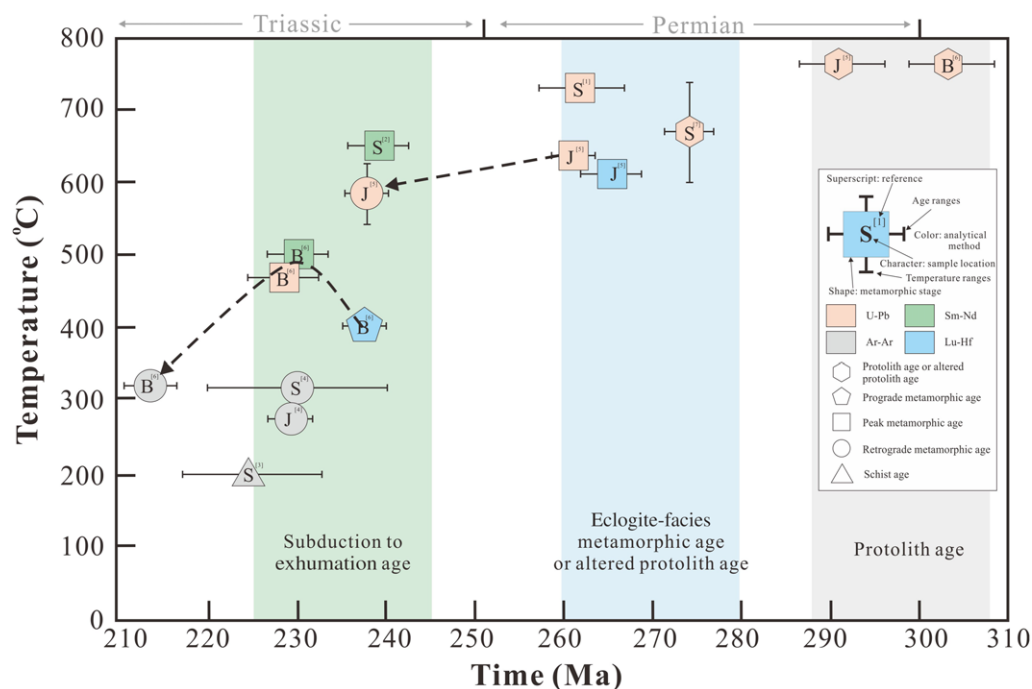


**Fig. 6.** The age distribution of the eclogite and schist in the Lhasa terrane. The letter inside the  $P$ - $T$  symbols gives the sample location: S, Sumdo; J, Jilang; B, Bailang. Indicated references are: [1] Yang *et al.* (2009); [2] Zeng *et al.* (2009); [3] H.Q. Li *et al.* (2009); [4] Li *et al.* (2011); [5] Cheng *et al.* (2012); [6] Cheng *et al.* (2015); [7] Weller *et al.* (2016).

a lower intercept age of  $273.6 \pm 2.8$  Ma (MSWD = 1.5) in a Tera-Wasserburg diagram with an uncorrected common Pb dataset. This age is interpreted as the minimum age for the eclogite-facies metamorphism, indicating new zircon growth interpreted to be due to the recrystallization of magmatic protolith zircons by subsolidus dissolution–precipitation mechanisms under the influence of metamorphic fluids introduced during subduction. The latter interpretation is based on the following four arguments: (1) both low-grade (biotite and chlorite) and high-grade metamorphic minerals (garnet and omphacite) were found included in zircon; (2) CL images of the analysed zircons exhibit irregular and diffuse mosaic-type patterns; (3) the Th/U ratios of the zircons range from 0.01 to 1.62, which indicate their metamorphic and igneous characteristics; and (4) the zircon grains contained a highly variable contents of high field-strength elements (HFSE), such as Hf (8484–18 722 ppm) and Yb (38–1279 ppm), characteristic of a metamorphic (low values) and an igneous (high values) origin of the zircons.

Using whole-rock (WR)–garnet–omphacite Sm–Nd analyses from 13 eclogite samples of the Sumdo area, Zeng *et al.* (2009) obtained an isochron age of

$239.0 \pm 3.5$  Ma with an initial  $^{143}\text{Nd}/^{144}\text{Nd}$  value of 0.512742 (Fig. 6; Table 1), interpreted as the age of eclogite-facies metamorphism. On the other hand, using retrogressed eclogite samples from the same outcrop, Z.L. Li *et al.* (2009) obtained different Nd isotope compositions ( $\epsilon_{\text{Nd}(t)}$  ranges from 7.4 to 8.2) and a  $305.5 \pm 50$  Ma (MSWD = 1.56) isochron age with large errors from the same eclogites, interpreted to be the protolith age of the eclogite, based on a c. 40 Ma time span between the Sm–Nd ages and the published zircon U–Pb ages in the same area. However, this isochron age is only obtained on Sm–Nd data from WR analyses with narrow  $^{143}\text{Nd}/^{144}\text{Nd}$  (0.5130–0.5132) and  $^{147}\text{Sm}/^{144}\text{Nd}$  (0.18–0.27) intervals, which cannot result in a reliable isochron age.

White mica from quartzite and retrogressed eclogites, as well as amphibole from eclogite of the Sumdo area, were analysed by the  $^{40}\text{Ar}/^{39}\text{Ar}$  method to constrain the time of exhumation (H.Q. Li *et al.* 2009, 2011).  $^{40}\text{Ar}/^{39}\text{Ar}$  plateau ages of 241–224 Ma for white mica and c. 235 Ma for amphibole from retrogressed eclogite were measured, and indicate that the eclogite and associated mica quartzite were exhumed back to shallow crustal levels during the middle Triassic.

### *Jilang phengite eclogites*

Zircon U–Pb ages and a corresponding garnet Lu–Hf isochron age were obtained for the same sample of eclogite from the Jilang area (Cheng *et al.* 2012). The Lu–Hf age of  $265.9 \pm 1.1$  Ma (MSWD = 1.8) was based on a three-point isochron defined by WR + garnet + omphacite. Analysed zircon crystals from eclogite were subhedral, transparent and colourless, with only a few solid inclusions. Most zircon grains showed a CL bright homogeneous core surrounded by a dark rim. SIMS and LA–ICP–MS analysis of the zircon cores showed high U and Th contents, high Th/U ratios, enriched HREEs patterns, and yielded  $^{206}\text{Pb}/^{238}\text{U}$  apparent ages of  $329.6 \pm 22.8$  to  $281.9 \pm 16.4$  Ma, with a weighted mean age of  $290.6 \pm 6.2$  Ma (MSWD = 1.1) in the Tera–Wasserburg diagram and a  $^{207}\text{Pb}$  corrected dataset. These grain cores were interpreted as magmatic zircon crystals that had experienced different degrees of solid-state recrystallization. The zircon rim domains are unzoned, containing inclusions of garnet, omphacite and quartz, and are interpreted to represent metamorphic overgrowth rims. They exhibit flat HREE patterns with low Th/U ratios ( $\leq 0.09$ , with an average of 0.04). The isotope analyses of the zircons yielded relatively imprecise U–Th–Pb data due to their low U, Th and Pb contents, and relatively high common Pb content. SIMS analyses of the zircon overgrowth rims revealed two apparent  $^{206}\text{Pb}/^{238}\text{U}$  age peaks of  $261.2 \pm 3.1$  and  $238.1 \pm 3.2$  Ma (Fig. 6). These zircon overgrowth ages are interpreted to reflect the pulsed growth of zircon during eclogite-facies metamorphism and later retrogression (Cheng *et al.* 2012). This interpretation is also supported by the  $230 \pm 2$  Ma  $^{40}\text{Ar}/^{39}\text{Ar}$  white mica isochron ages in the Jilang eclogite (Li *et al.* 2011).

### *Bailang glaucophane eclogites*

Zircons in glaucophane eclogite samples from the Bailang area occur as transparent and colourless, anhedral to euhedral crystals. CL images show an unzoned or sector-zoned core, surrounded by a thin overgrowth rim ( $<30$   $\mu\text{m}$ ) that contains inclusions of garnet, omphacite and phengite. The zircon cores have high Th/U ratios (0.24–2.33), HREE enrichment and negative Eu anomalies. LA–ICP–MS analyses yield a broad range of ages between 320 and 270 Ma, with a weighted mean  $^{206}\text{Pb}/^{238}\text{U}$  age of  $304 \pm 5$  Ma (MSWD = 5.0) (Fig. 6; Table 1). The zircon rims have very low U and radiogenic Pb contents, and flat HREE patterns with no negative Eu anomalies. Apparent ages are between 245 and 215 Ma, defining a lower intercept age of  $227.4 \pm 6.4$  Ma (MSWD = 1.8) (Fig. 6) (Cheng *et al.* 2015).

Garnet, omphacite and the corresponding WR of Bailang glaucophane eclogite was analysed by the Lu–Hf and Sm–Nd methods (Cheng *et al.* 2015). Garnet fractions have rather low Hf contents (*c.* 0.1 ppm), producing less precise Hf isotope analyses than the WR. Lu–Hf and Sm–Nd isochron ages were constrained by Savillex-digested WR, bomb-digested WR, garnet and/or omphacite aliquots (Cheng *et al.* 2008). Six garnet fractions combined with two WRs yielded a Lu–Hf age of  $238.1 \pm 3.6$  Ma (MSWD = 5.4) and a corresponding Sm–Nd age of  $230.0 \pm 4.7$  Ma (MSWD = 0.3), with initial epsilon values calculated for their metamorphic ages of  $\epsilon_{\text{Hf}} (t = 240 \text{ Ma}) = +11.5$  and  $\epsilon_{\text{Nd}} (t = 230 \text{ Ma}) = +6.5$  (Cheng *et al.* 2015).

Amphibole  $^{40}\text{Ar}/^{39}\text{Ar}$  analyses showed a poorly weighted plateau age of  $200.5 \pm 7.2$  Ma for eclogite (Fig. 6). As the maximum temperature of the Bailang eclogite equals or exceeds the Ar closure temperature of *c.*  $450 \pm 50^\circ\text{C}$ , this means that no significant excess Ar has been incorporated at or after the time of initial closure of the isotopic system in amphibole. Cheng *et al.* (2015) proposed that this  $200.5 \pm 7.2$  Ma age is the minimum time for the epidote–amphibolite-facies metamorphism that post-dates the eclogite formation.

## Discussion

### *The geological significance of the Sumdo (U) HP metamorphic belt in the Lhasa terrane*

The Sumdo Complex is an east–west-trending, high-pressure (HP) and ultrahigh-pressure (UHP) metamorphic belt that extends for over 100 km across the middle part of the Lhasa terrane in southern Tibet (Fig. 1). This eclogite-bearing complex was interpreted to have formed in a Permian–Triassic subduction zone (Yang *et al.* 2006), leading to a reinterpretation of the tectonic evolution of the entire Lhasa terrane. The latter was previously considered to be a single tectonic domain that drifted away from Gondwana during the closure of the Palaeo-Tethys Ocean to ultimately collide with the SE Asian plate margin. In this model, the Lhasa terrane formed a composite tectonic unit in which the northern and southern Lhasa segments (sub-terrane) were united together. As such, in this early model, the Lhasa terrane formed the leading edge of the amalgamated SE Asian plate boundary that was formed prior to the Cenozoic collision with India. As such, the tectonometamorphic evolution of the Sumdo (U)HP metamorphic terrane, located in-between the northern and southern segments of the Lhasa terrane, forms a key element in our understanding of the Himalayan–Tibetan orogeny (Yin & Harrison 2000; Zhu *et al.* 2011b; Zhang *et al.* 2014).

In order to constrain the physical conditions of the metamorphic processes that formed the eclogites of the Sumdo Complex, two different thermodynamic techniques were applied to eclogites, associated blueschists and garnet-bearing mica schists in order to calculate the  $P$ – $T$  path/ $P$ – $T$  conditions of these metamorphic rocks. With conventional garnet–clinopyroxene  $\text{Fe}^{2+}$ –Mg exchange geothermometry (Krogh Ravna 2000) combined with garnet–clinopyroxene–phengite– $\text{SiO}_2$  geobarometry (Krogh Ravna & Terry 2004),  $P$ – $T$  conditions of c. 27 kbar, 730°C (Yang *et al.* 2009) and 33–39 kbar, 760–800°C (Zhang *et al.* 2011) were calculated for the Sumdo phengite eclogites, and 34–38 kbar, 753–790°C for the Jilang eclogite (Fig. 6) (Cheng *et al.* 2012). The latter  $P$ – $T$  results, illustrated by yellow markers in Figure 4, are indicative of MT HP and UHP eclogite-facies conditions (Wei *et al.* 2013). However, using the alternative isopleths  $P$ – $T$  constraint method for phase-equilibrium calculations in Thermocalc (Powell *et al.* 1998) and/or Theriak/Domino (de Capitani & Petrakakis 2010),  $P$ – $T$  conditions of c. 30–32 kbar, 610–620°C and 29 kbar, 610°C (Cheng *et al.* 2012; Yang *et al.* 2014; Huang *et al.* 2015) were calculated for the phengite and glaucophane eclogites collected in the same outcrops in the Sumdo and Jilang areas, respectively. The latter  $P$ – $T$  conditions are also visualized in Figure 4 (as green hexagons marked with symbols S and J). According to the subclassification system of Wei *et al.* (2013), the latter  $P$ – $T$  conditions are, however, characteristic of LT HP and UHP eclogite-facies conditions. This means that, following the subclassification system of Wei *et al.* (2013), two different  $P$ – $T$  domains can be calculated in  $P$ – $T$  space for the same eclogite body/bodies: for example, representing LT v. MT eclogite-facies conditions, which usually correspond to the Alpine type of cold subduction and the Pacific type of warm collision, respectively. It will be clear that such alternative interpretations will create a lot of ‘confusion’, especially if one combines this ‘confusion’ with the following important questions. These questions are: does the reported spread in calculated  $P$ – $T$  conditions, illustrated in Figure 4 (including the other data points taken from the literature), represent: (1) one orogenic event, implying a tectonic scenario that starts with oceanic subduction followed by continental collision? (2) Do the eclogites represent different metabasic bulk-rock types formed in different tectonic settings? (3) Can the range in  $P$ – $T$  conditions be treated as a mix of  $P$ – $T$  conditions that were formed at different depths of the subduction system but became juxtaposed together during exhumation? Or (4) does this range of calculated  $P$ – $T$  conditions ‘originate’ from inconsistencies in the application of different thermodynamic methods?

It is not difficult to find out that  $P$ – $T$  conditions calculated by the conventional geothermobarometric technique are often much higher than those calculated using phase-equilibrium calculations. A good example of this is illustrated by the work of Wei *et al.* (2009), who published pseudosections calculated for an eclogite with a MORB bulk-rock chemical composition. This was done to simulate the intersection point between the garnet–clinopyroxene (GC) geothermometer(s) and the garnet–clinopyroxene–phengite (GCP) geobarometer, and thus to test the applicability of this method to eclogites containing a different mineral assemblage. The results clearly demonstrated that the position in  $P$ – $T$  space of the isopleth lines of Si (in phengite) and Ca, Mg, Fe (in garnet and omphacite) are strongly controlled not only by the  $P$ – $T$  conditions, but also by the bulk-rock composition and/or available mineral assemblages. As for the GC geothermometer, at least 10 different calibrations have been applied to calculate the temperature for eclogite (e.g. Ellis & Green 1979; Powell 1985; Krogh Ravna 1988, 2000; Krogh Ravna & Terry 2004). The application of all these geothermometric techniques results in a big error (100–200°C wide) when applied to the same sample/mineral assemblage. Powell & Holland (2008) considered that the biggest problem with the application of the GC geothermometer to eclogites is that the initial experiments were carried out under a temperature range of 600–1500°C (and excluding side-effects introduced by (non-) linear extrapolation of the experimental results), making it suitable for application to eclogites formed under medium- to high-temperature conditions, (i.e. conforming to the kyanite-bearing eclogite: Wei *et al.* 2009), but not for LT eclogites.

The HP and UHP conditions of eclogite from the Sumdo and Jilang areas are always determined by the high Si content (c. 3.6 pfu) in phengite (Zhang *et al.* 2011; Cheng *et al.* 2012). However, the Si content in phengite is controlled not only by the  $P$ – $T$  conditions but also by the available mineral assemblage and/or the bulk-rock composition (Massonne & Schreyer 1989; Wei & Powell 2003, 2004). This is exemplified for the case of Si = 3.4–3.5 pfu in phengite. For a kyanite-bearing eclogite, this indicates >29 kbar (UHP metamorphic conditions), but for a glaucophane-bearing eclogite this indicates only 22–26 kbar and LT conditions within the stability field of lawsonite (Wei *et al.* 2009). Recalculations of the metamorphic conditions of the Jilang eclogite, using the highest Mg content ( $X_{\text{mg}}$ ) in garnet (0.3) intersecting the highest Si isopleth of 3.6 pfu in phengite in a pseudosection made with Theriak/Domino, results in  $P$ – $T$  conditions of c. 29 kbar and 610°C, clearly within the LT eclogite-facies field of Wei *et al.* (2009), but around 150°C lower than the temperature calculated using



conventional geothermobarometric techniques (Cheng *et al.* 2012). So, it is worth noting that the  $P$ – $T$  results calculated from the pseudosection work may also result in unignorable errors due to the effects of inappropriate choices of bulk-rock composition, mineral mode and thermodynamic dataset.

The above-discussed  $P$ – $T$  results, summarized in Figure 4 by the green symbols within the EP–EC field, are indicative of LT HP and UHP metamorphic conditions revealing fast subduction and related exhumation processes formed in a typical intra-oceanic subduction-zone setting. However, when the LT–HP metamorphic conditions of the lawsonite-bearing glaucophane eclogite of the Bailang area (25–27 kbar, 465–503°C; Cheng *et al.* 2015) are also added to the overall  $P$ – $T$  picture of Figure 4 (green square and green pentagon in the Lws–Ec field), it becomes clear again that it is no longer possible to eliminate the option that the Sumdo eclogites in the south-central part of the Lhasa Block can be derived from distinct slices of subducted blocks that were exhumed from different parts of the subduction zone and subsequently juxtaposed together during exhumation. Consequently, more systematic investigations of the (metamorphic) petrology and  $P$ – $T$  evolution of the different types of eclogites present within the Sumdo (U)HP terrane of the Lhasa Block are still needed to further constrain the metamorphic evolution and tectonic processes of the suture zone.

### *The interpretation of the metamorphic and their protolith formation ages of the eclogites in the Sumdo (U)HP metamorphic belt*

The Sumdo eclogite-bearing complex is thought to form the remnants of an oceanic floor that was formed during the Carboniferous, followed by closure in an intra-oceanic supra-subduction-zone environment that was established in the Permian–Triassic period, but prior to the final accretion of the North and South Lhasa terranes (Chen *et al.* 2009; Yang *et al.* 2009). The eclogites with MORB and OIB protolith affinity (Fig. 5) underwent metamorphism at a low geothermal regime of 6–10°C km<sup>−1</sup> (Yang *et al.* 2014; Cheng *et al.* 2015), indicating a typical oceanic subduction-zone environment, which is interpreted to be a remnant of the Palaeo-Tethys oceanic crust. This is similar to the UHP eclogites from the Limousin area in France (Berger *et al.* 2010), and the western Tianshan and northern Qilian in China (Song *et al.* 2013; Zhang *et al.* 2013), but quite different from the UHP rocks with a continental origin (Zheng 2012).

SHRIMP U–Pb zircon ages of 262 ± 5 Ma from the Sumdo eclogites (Yang *et al.* 2009), LA-ICP-MS

ages of 261 ± 3–238 ± 3 Ma from the Jilang eclogites and SIMS ages of 227 ± 6 Ma from the Bailang eclogites were interpreted to estimate eclogite-facies metamorphism during subduction (Fig. 6) (Cheng *et al.* 2012, 2015). The whole rock (WR)–garnet–omphacite Lu–Hf ages of 265.9 ± 1.1 Ma (Jilang eclogite) and 238.1 ± 3.6 Ma (Bailang eclogite) were interpreted as the age of garnet crystallization during high-pressure eclogite-facies metamorphism and a mixture of the ages of relatively old garnet cores and young garnet rims, respectively (Cheng *et al.* 2012, 2015). A 239 ± 3.5 Ma WR–garnet–omphacite Sm–Nd isochron age (Zeng *et al.* 2009) has a c. 20 myr time difference to the zircon U–Pb ages from the Sumdo eclogite; it is, however, comparable with a 238 ± 3 Ma zircon age and a 238.1 ± 3.6 Ma Lu–Hf age for the Bailang eclogite, but 10 myr older than a 230 ± 4.7 Ma WR–garnet–omphacite Sm–Nd isochron age for the Bailang eclogite. In summary, the published eclogite-facies metamorphic ages of the eclogites from the Lhasa terrane, obtained with different isotopic methods, range from 266 to 227 Ma, implying a large time span of 40 myr for subduction (Fig. 6). Does this time span reflect long-term subduction at very low subduction rates or diachronous subduction with subduction and exhumation of distinct slices from different depths at different times? Weller *et al.* (2016) performed a *in situ* SHRIMP analysis of zircons from the Sumdo eclogite that connected the zircon ages with the mineralogical evaluation to illustrate the  $P$ – $T$ –time ( $t$ ) path of eclogite, and yielded a 274 ± 3 Ma lower intercept age in the Tera–Wasserburg diagram. On the basis of phase-equilibrium calculations in the NCKFMASHTO system and the Zr content of Ti-bearing minerals, this age is interpreted to date the recrystallization of magmatic protolith zircon during prograde metamorphism by subsolidus dissolution–precipitation under the influence of metamorphic fluids (Rubatto *et al.* 2008). The growth of zircon is strongly affected by the formation and consumption of Zr-bearing minerals such as rutile and ilmenite in eclogite, making the interpretation of zircon ages highly variable. From mass-balance considerations of the Zr budget, Kohn *et al.* (2015) suggested that most zircons from eclogites grow during retrogression, with the breakdown of rutile and ilmenite and/or titanite being the Zr source(s). However, this does not account for the Zr contribution from the primary igneous zircons that permitted the recrystallization of zircon during prograde metamorphism or the dissolution of Zr-bearing magmatic phases such as ilmenite (Bingen *et al.* 2001; St-Onge *et al.* 2013; Beckman *et al.* 2014). The reinterpretation of the Permian zircon ages (262 ± 5 Ma and 261 ± 3 Ma) of eclogites from the Sumdo and Jilang areas is still made with uncertainty. It may represent the eclogite-facies metamorphism stated in the

literature (Yang *et al.* 2009; Cheng *et al.* 2012) and can also, alternatively, be interpreted as reflecting age mixing between the protolith formation and the prograde metamorphism of eclogites for the following two reasons: (1) the low content of Th and radioactive lead ( $Pb^* < 1$  ppm) and the high content of common Pb make the analysed data highly uncertain and ambiguous; and (2) none of the single-grain ages that these two Permian mean ages were calculated from is concordant. However, the  $265.9 \pm 1.1$  Ma WR–omphacite–garnet Lu–Hf isochron age can be attributed to the deduction of the eclogite-facies metamorphism in the Permian on the basis of the following three reasons: (1) A low-pressure tabletop-digested technique (Cheng *et al.* 2008) with a careful hand-picking procedure has been used to prevent the dissolution of Hf-rich phases like rutile and zircon. (2) The results from isotope dilution analysis are in good agreement with the Lu/Hf ratios of garnets obtained from *in situ* LA-ICP-MS studies, indicating that the contamination of garnet by zircon inclusions was minor. (3) The recalculated peak metamorphic temperature (c. 610°C in Fig. 4) of

the Jilang eclogite is lower than the closure temperature of the Lu–Hf system in garnet ( $>680^\circ\text{C}$ ; Scherer *et al.* 2000), making a close isotope system during metamorphism.

Considering these data in context with the 230–220 Ma  $^{40}\text{Ar}/^{39}\text{Ar}$  retrogression ages from eclogites and an associated schist (Fig. 6) (H.Q. Li *et al.* 2009, 2011; Cheng *et al.* 2012), we conclude that the diachronous subduction by different oceanic slices during 245–225 Ma is more likely to reflect the main closure of the Palaeo-Tethys Ocean, which led to the amalgamation of North and South Lhasa (Fig. 7). The initiation of the opening of the Palaeo-Tethys Ocean could be traced back to the early Permian ( $>280$  Ma) and the beginning of the oceanic crust subduction, represented by the Jilang eclogite, with the eclogite-facies metamorphic depth to the late Permian (c. 266 Ma). A slice of oceanic crust hosting the Sumdo eclogite experienced deep subduction, with UHP eclogite-facies metamorphism at c. 240 Ma and exhumation at 230 Ma. A successive slice hosting the Bailang eclogite that has an OIB affinity experienced HP–LT eclogite-facies

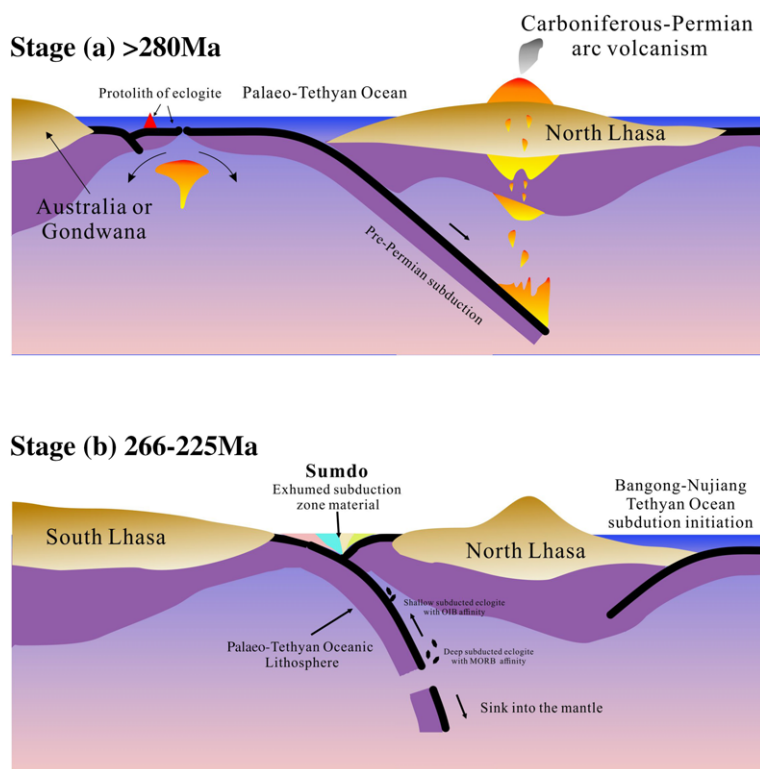


**Fig. 7.** Schematic illustrations of the tectonic evolution of the eclogites from the Lhasa terrane. Stage (a) shows the origin of the  $>280$  Ma eclogite protolith and the formation of the Carboniferous–Permian volcanic rocks distributed in the North Lhasa terrane. Stage (b) shows the subduction and exhumation of the eclogites.

metamorphism at 230 Ma at a shallower level. The Palaeo-Tethys Ocean did not close before 210 Ma, based on  $^{40}\text{Ar}/^{39}\text{Ar}$  plateau ages (Cheng *et al.* 2015), a notion further supported by the existence of a post-orogenic granite in Gongdise, in the South Lhasa terrane (Li *et al.* 2003; Liu *et al.* 2006; Zhang *et al.* 2007).

### *The tectonic evolution of the Sumdo Complex*

The Tibetan Plateau, Earth's largest active continent–continent collisional orogen, has received plenty of scientific investigation on magmatism (J. Zhang *et al.* 2012; Hébert *et al.* 2014), geophysics (Zhao *et al.* 2014; Xu *et al.* 2015), palaeomagnetism (Klootwijk 2013; Li *et al.* 2016) and metamorphism (Cheng *et al.* 2012; Zhang *et al.* 2014) to improve our understanding of the evolution of this giant orogenic belt. Continuous consumption of the Tethys Ocean involved accretion of multiple intra-oceanic arcs and microcontinents prior to the eventual continent–continent collision (Yin & Harrison 2000), resulting in the accretion of several HP metamorphic rock-bearing terranes, such as those of Lhasa, Qiangtang and Amdo prior to the collision of the Indian and Eurasian plates (Yang *et al.* 2009; Zhai *et al.* 2011; Z.M. Zhang *et al.* 2012; Zhu *et al.* 2013). Various models have been proposed for the origin and evolution of the Tibetan Plateau resulting from multiple collision events between these terranes (Yin & Harrison 2000; Gehrels *et al.* 2011; Zhu *et al.* 2013; Zhang *et al.* 2014).

The Lhasa terrane occupies an important position in the Himalayan–Tibetan orogeny. Therefore, its origin and evolution are the keys to building tectonic models of this orogen. However, the origin of the Lhasa terrane is still controversial. Yin & Harrison (2000) initially considered it as an integral fragment rifted from the northern margin of Gondwana at Paleozoic–Early Mesozoic time, which has been confirmed by systematic U–Pb dating of detrital zircons from pre-Tertiary strata in the Himalayan–Tibetan orogen (Gehrels *et al.* 2011). From new data on the distribution of major tectonic boundaries, basement rocks and their sedimentary cover, magmatic suites, and detrital zircons from Paleozoic metasedimentary rocks, Zhu *et al.* (2011a) proposed an Australia affinity for the Lhasa terrane. The late Devonian granitoids at the southern margin of the Lhasa terrane may represent an extensional magmatic event associated with its rifting, ultimately resulting in the opening of the Palaeo-Tethys Ocean. Proposing a tectonic model to explain the origin of the Lhasa terrane is far beyond the current geochemical and geochronological level of knowledge on eclogites from the Sumdo Complex. Nevertheless, >280 Ma eclogite protolith ages from zircon cores and MORB or OIB-like geochemical features

indicate that the North Lhasa terrane has rifted away from its ‘motherland’ and the Palaeo-Tethys Ocean formed before early Permian time (Fig. 7) (Yang *et al.* 2009; Cheng *et al.* 2012, 2015). During subduction between the South and North Lhasa terranes, LT HP–UHP metamorphism proceeded, with Early Triassic exhumation of the created eclogites (266–225 Ma: Fig. 7). The final collision of the South and North Lhasa terranes may also assist in the subduction initiation of the Bangong–Nujiang Tethys Ocean in the north (Zhu *et al.* 2013). A medium-pressure metamorphic belt present along a length of up to 500 km between the South and North Lhasa terranes, at 225–210 Ma, has also been reported from this belt (Dong *et al.* 2011; Zhang *et al.* 2014). This Triassic medium-pressure metamorphism is associated with widespread granitic magmatism with a geochemical affinity to post-collisional plutons (Li *et al.* 2003; Zhang *et al.* 2007; Zhu *et al.* 2011b); it followed the closure of the Palaeo-Tethys Ocean, which is concordant with the Early Triassic Andean-type subduction reflected in the integration of the Lhasa terrane.

### Conclusions

From reviewing the mineralogical, petrological, geochemical and geochronological data of (U)HP rocks from the Sumdo, Jilang and Bailang area, together forming the Sumdo Complex of the Lhasa terrane, the following conclusions have been drawn:

- Eclogites of the Sumdo terrane have experienced low-temperature (LT) and high-pressure (HP) to ultrahigh-pressure (UHP) metamorphic conditions, revealing a fast subduction and exhumation process in a typical intra-oceanic subduction-zone setting. Most probably, distinct slices of subducted blocks, derived from different depths in the subduction zone, were juxtaposed together during exhumation.
- The age of the eclogite-facies metamorphism in the Sumdo Complex of the Lhasa terrane is most likely from late Permian (c. 260 Ma) to early Triassic (245–225 Ma), and may have been caused by different portions of oceanic crust recording metamorphic age at different depths.
- The opening of the Palaeo-Tethys Ocean, located in-between the two segments that together form the Lhasa terrane, was initiated prior to c. 280 Ma. Ultimate closure and final collision of the two terranes (called the northern and southern segments), which together formed the Lhasa terrane, was not earlier than 210 Ma. The latter may have been assisted by the initial subduction of the Bangong–Nujiang Tethys Ocean in the north.



**Acknowledgements** Guest editor Lifei Zhang, Jana Kotkova and two anonymous reviewers are thanked for their constructive comments that considerably improved the early version of this manuscript.

**Funding** This research is financially supported by the National Natural Science Foundation of China (grant Nos 41572051, 41630207 and 41502039 to C. Zhang, J.X. Zhang and T. Shen, respectively), the Chinese Academy of Geological Sciences (grant No. YYWF201702 to C. Zhang) and the Basic Geological Survey Program of China of the China Geological Survey (grant No. DD20160022-01 to C. Zhang).

## References

- ALLEGRE, C.J., COURTILLOT, V. ET AL. 1984. Structure and evolution of the Himalaya–Tibet orogenic belt. *Nature*, **307**, 17–22.
- BECKMAN, V., MÖLLER, C., SÖDERLUND, U., CORFU, F., PAL-LON, J. & CHAMBERLAIN, K.R. 2014. Metamorphic zircon formation at the transition from gabbro to eclogite in Trollheimen–Surnadalen, Norwegian Caledonides. In: CORFU, F., GASSER, D. & CHEW, D.M. (eds) *New Perspectives on the Caledonides of Scandinavia and Related Areas*. Geological Society, London, Special Publications, **390**, 403–424, <https://doi.org/10.1144/SP390.26>
- BERGER, J., FEMENIAS, Q., OHNSTETTER, D., BRUGUIER, O., PLISSART, G., MERCIER, J.-C.C. & DEMAIFFE, D. 2010. New occurrence of UHP eclogites in Limousin (French Massif Central): Age, tectonic setting and fluid–rock interactions. *Lithos*, **118**, 365–382.
- BERNARD-GRIFFITHS, J. & CORNICHE, J. 1985. Origin of eclogites from South Brittany, France: a Sm–Nd isotopic and REE study. *Chemical Geology: Isotope Geoscience Section*, **52**, 185–201.
- BINGEN, B., AUSTRHEIM, H. & WHITEHOUSE, M. 2001. Ilmenite as a source for zirconium during high-grade metamorphism? Textural evidence from the Caledonides of western Norway and Implications for zircon geochronology. *Journal of Petrology*, **42**, 355–375.
- CARSWELL, D.A. & CUTHBERT, S.J. 2003. Ultrahigh pressure metamorphism in the Western Gneiss Region of Norway. In: CARSWELL, D.A. & COMPAGNONI, R. (eds) *Ultrahigh Pressure Metamorphism*. EMU Notes in Mineralogy, **5**, 51–73.
- CHEN, M., TIAN, Z.L., ZHANG, C., YANG, J.S. & HUANG, J. 2015. Phase equilibrium modeling for metamorphic evolution of garnet-bearing mica–quartz schist in Sumdo UHP metamorphic belt, Lhasa Block. *Geology in China*, **42**, 1572–1587 [in Chinese with an English abstract].
- CHEN, S., YANG, J., LI, Y. & XU, X. 2009. Ultramafic blocks in Sumdo region, Lhasa block, Eastern Tibet plateau: an ophiolite unit. *Journal of Earth Science*, **20**, 332–347.
- CHENG, H., KING, R.L., NAKAMURA, E., VERVOORT, J.D. & ZHOU, Z. 2008. Coupled Lu–Hf and Sm–Nd geochronology constrains garnet growth in ultra-high-pressure eclogites from the Dabie orogen. *Journal of Metamorphic Geology*, **26**, 741–758.
- CHENG, H., ZHANG, C., VERVOORT, J.D., LU, H., WANG, C. & CAO, D. 2012. Zircon U–Pb and garnet Lu–Hf geochronology of eclogites from the Lhasa Block, Tibet. *Lithos*, **155**, 341–359.
- CHENG, H., LIU, Y., VERVOORT, J.D. & LU, H. 2015. Combined U–Pb, Lu–Hf, Sm–Nd and Ar–Ar multi-chronometric dating on the Bailang eclogite constrains the closure timing of the Paleo-Tethys Ocean in the Lhasa terrane, Tibet. *Gondwana Research*, **28**, 1482–1499.
- CHOPIN, C. 1984. Coesite and pure pyrope in high-grade blueschists of the Western Alps – a 1st record and some consequences. *Contributions to Mineralogy and Petrology*, **86**, 107–118.
- CHOPIN, C. 2003. Ultrahigh-pressure metamorphism: tracing continental crust into the mantle. *Earth and Planetary Science Letters*, **212**, 1–14.
- CONNOLLY, J.A.D. 2005. Computation of phase equilibria by linear programming: a tool for geodynamic modeling and its application to subduction zone decarbonation. *Earth and Planetary Science Letters*, **236**, 524–541.
- DE CAPITANI, C. & PETRAKAKIS, K. 2010. The computation of equilibrium assemblage diagrams with Theriak/Domino software. *American Mineralogist*, **95**, 1006–1016.
- DONG, X., ZHANG, Z., LIU, F., WANG, W., YU, F. & SHEN, K. 2011. Zircon U–Pb geochronology of the Nyainqentanglha Group from the Lhasa terrane: new constraints on the Triassic orogeny of the south Tibet. *Journal of Asian Earth Sciences*, **42**, 732–739.
- ELLIS, D.J. & GREEN, D.H. 1979. An experimental study of the effect of Ca upon the garnet clinopyroxene Fe–Mg exchange equilibria. *Contributions to Mineralogy and Petrology*, **71**, 13–22.
- ERNST, W.G. & LIOU, J.G. 1995. Contrasting plate-tectonic styles of the Qinling–Dabie–Sulu and Franciscan metamorphic belts. *Geology*, **23**, 353–356.
- ERNST, W.G. & LIOU, J.G. 2008. High- and ultrahigh-pressure metamorphism–past results, future prospects. *American Mineralogist*, **93**, 1771–1786.
- ERNST, W.G., HACKER, B.R. & LIOU, J.G. 2007. Petrotectonics of ultrahigh-pressure crustal and upper-mantle rocks – Implications for Phanerozoic collisional orogens. In: SEARS, J.W., HARMS, T.A. & EVENCHICK, C.A. (eds) *Whence the Mountains? Inquiries into the Evolution of Orogenic Systems: A Volume in Honor of Raymond A. Price*. Geological Society of America, Special Papers, **433**, 27–50.
- FERRARI, O.M., HOCHARD, C. & STAMPFLI, G.M. 2008. An alternative plate tectonic model for the Palaeozoic–Early Mesozoic Palaeotethyan evolution of Southeast Asia (Northern Thailand–Burma). *Tectonophysics*, **451**, 346–365.
- GEHRELS, G., KAPP, P. ET AL. 2011. Detrital zircon geochronology of pre-Tertiary strata in the Tibetan–Himalayan orogen. *Tectonics*, **30**, TC5016.
- GUYNN, J.H., KAPP, P., PULLEN, A., HEIZLER, M., GEHRELS, G. & DING, L. 2006. Tibetan basement rocks near Amdo reveal ‘missing’ Mesozoic tectonism along the Bangong suture, central Tibet. *Geology*, **34**, 505–508.
- GUYNN, J.H., KAPP, P., GEHRELS, G.E. & DING, L. 2012. U–Pb geochronology of basement rocks in central Tibet and paleogeographic implications. *Journal of Asian Earth Sciences*, **43**, 23–50.

- HÉBERT, R., GUILMETTE, C., DOSTAL, J., BEZARD, R., LESAGE, G., BÉDARD, É. & WANG, C. 2014. Miocene post-collisional shoshonites and their crustal xenoliths, Yarlung Zangbo Suture Zone southern Tibet: geodynamic implications. *Gondwana Research*, **25**, 1263–1271.
- HUANG, J., TIAN, Z.L., ZHANG, C., YANG, J.S. & CHEN, M. 2015. Metamorphic evolution of Sumdo eclogite in Lhasa Block of the Tibetan Plateau: phase equilibrium in NCKMnFMASHTO system. *Geology in China*, **42**, 1559–1571 [in Chinese with an English abstract].
- KAPP, P., DECELLES, P.G., GEHRELS, G.E., HEIZLER, M. & DING, L. 2007. Geological records of the Lhasa–Qiangtang and Indo–Asian collisions in the Nima area of central Tibet. *Geological Society of American Bulletin*, **119**, 917–932.
- KLOOTWIJK, C. 2013. Middle–Late Paleozoic Australia–Asia convergence and tectonic extrusion of Australia. *Gondwana Research*, **24**, 5–54.
- KOHN, M.J., CORRIE, S.L. & MARKLEY, C. 2015. The fall and rise of metamorphic zircon. *American Mineralogist*, **100**, 897–908.
- KROGH RAVNA, E. 1988. The garnet clinopyroxene Fe–Mg geothermometer: a reinterpretation of existing experimental data. *Contributions to Mineralogy and Petrology*, **99**, 44–48.
- KROGH RAVNA, E. 2000. The garnet–clinopyroxene Fe<sup>2+</sup>–Mg geothermometer: an updated calibration. *Journal of Metamorphic Geology*, **18**, 211–219.
- KROGH RAVNA, E. & TERRY, M.P. 2004. Geothermobarometry of UHP and HP eclogites and schists – an evaluation of equilibria among garnet–clinopyroxene–kyanite–phengite–coesite/quartz. *Journal of Metamorphic Geology*, **22**, 579–592.
- LEEDER, M.R., SMITH, A.B. & JIXIANG, Y. 1988. Sedimentology, palaeoecology and palaeoenvironmental evolution of the 1985 Lhasa to Golmud geotraverse. *Philosophical Transactions of the Royal Society of London. Series A, Mathematical and Physical Sciences*, **327**, 107–143.
- LI, C., WANG, T.W., LI, H.M. & ZENG, Q.G. 2003. Discovery of Indosinian megaporphyritic granodiorite in the Gangdise area: evidence for the existence of Paleogangdise. *Geological Bulletin of China*, **22**, 364–366 [in Chinese with an English abstract].
- LI, C., ZHAI, Q.G., DONG, Y. & HUANG, X. 2006. Discovery of eclogite and its geological significance in Qiangtang area, central Tibet. *Chinese Science Bulletin*, **51**, 1095–1100 [in Chinese with an English abstract].
- LI, H.Q., XU, Z.Q., YANG, J.S., CAI, Z.H., CHEN, S.Y. & TANG, Z.M. 2009. Records of Indosinian orogenesis in Lhasa terrane, Tibet. *Journal of Earth Science*, **20**, 348–363.
- LI, H.Q., XU, Z.Q., YANG, J.S., TANG, Z.M. & YANG, M. 2011. Syn-collisional exhumation of Sumdo eclogite in the Lhasa Terrane, Tibet: evidences from structural deformation and <sup>40</sup>Ar–<sup>39</sup>Ar geochronology. *Earth Science Frontiers*, **18**, 66–78 [in Chinese with an English abstract].
- LI, Z.L., YANG, J.S., XU, Z.Q., LI, T.F., XU, X.Z., REN, Y.F. & ROBINSON, P.T. 2009. Geochemistry and Sm–Nd and Rb–Sr isotopic composition of eclogite in the Lhasa terrane, Tibet, and its geological significance. *Lithos*, **109**, 240–247.
- LI, Z.Y., DING, L., LIPPETT, P.C., SONG, P.P., YUE, Y.H. & VAN HINSBERGEN, D.J.J. 2016. Paleomagnetic constraints on the Mesozoic drift of the Lhasa terrane (Tibet) from Gondwana to Eurasia. *Geology*, **44**, 727–730.
- LIU, J.G., TSUJIMORI, T., ZHANG, S.G., KATAYAMA, I. & MARUYAMA, S. 2004. Global UHP metamorphism and continent subduction/collision: the Himalayan model. *International Geology Review*, **46**, 1–27.
- LIU, J.G., ERNST, W.G., SONG, S.G. & JAHN, B.M. 2009. Tectonics and HP–UHP metamorphism of northern Tibet – Preface. *Journal of Asian Earth Sciences*, **35**, 191–198.
- LIU, Q.S., JIANG, W., JIAN, P., YE, P.S., WU, Z.H. & HU, D. G. 2006. The zircon SHRIMP U–Pb age and petrochemical and geochemical features of Mesozoic muscovite monzogranite at Ningzhong, Tibet. *Acta Petrologica Sinica*, **22**, 463–652 [in Chinese with an English abstract].
- LIU, Y., LIU, H., THEYE, T. & MASSONNE, H.-J. 2009. Evidence for oceanic subduction at the NE Gondwana margin during Permo-Triassic times. *Terra Nova*, **21**, 195–202.
- MARUYAMA, S., LIU, J.G. & TERABAYASHI, M. 1996. Blueschists and eclogites of the world and their exhumation. *International Geology Review*, **38**, 485–594.
- MASSONNE, H.J. & SCHREYER, W. 1989. Stability field of the high pressure assemblage talc+phengite and two new phengite barometers. *European Journal of Mineralogy*, **1**, 391–410.
- METCALFE, I. 1996. Gondwanaland dispersion, Asian accretion and evolution of eastern Tethys. *Australian Journal of Earth Sciences*, **43**, 605–623.
- MO, X., NIU, Y., DONG, G., ZHAO, Z., HOU, Z., ZHOU, S. & KE, S. 2008. Contribution of syncollisional felsic magmatism to continental crust growth: a case study of the Paleogene Linzizong volcanic Succession in southern Tibet. *Chemical Geology*, **250**, 49–67.
- PAN, G., WANG, L. ET AL. 2012. Tectonic evolution of the Qinghai–Tibet Plateau. *Journal of Asian Earth Sciences*, **53**, 3–14.
- PHILIPPOT, P. & VAN ROERMUND, H.L.M. 1992. Deformation processes in eclogitic rocks – evidence for the rheological delamination of the oceanic-crust in deeper levels of subduction zones. *Journal of Structural Geology*, **14**, 1059–1077.
- POWELL, R. 1985. Regression diagnostics and robust regression in geothermometer/geobarometer calibration: the garnet–clinopyroxene geothermometer revisited. *Journal of Metamorphic Geology*, **3**, 231–243.
- POWELL, R. & HOLLAND, T.J.B. 2008. On thermobarometry. *Journal of Metamorphic Geology*, **26**, 155–179.
- POWELL, R., HOLLAND, T. & WORLEY, B. 1998. Calculating phase diagrams involving solid solutions via non-linear equations, with examples using THERMOCALC. *Journal of Metamorphic Geology*, **16**, 577–588.
- PULLEN, A., KAPP, P., GEHRELS, G.E., VERVOORT, J.D. & DING, L. 2008. Triassic continental subduction in central Tibet and Mediterranean-style closure of the Paleotethys Ocean. *Geology*, **36**, 351–354.
- RUBATTO, D., MÜNTENER, O., BARNHOORN, A. & GREGORY, C. 2008. Dissolution-reprecipitation of zircon at low-temperature, high-pressure conditions (Lanzo Massif, Italy). *American Mineralogist*, **93**, 1519–1529.
- SCHERER, E.E., CAMERON, K.L. & BLICHERT-TOFT, J. 2000. Lu–Hf garnet geochronology: closure temperature relative to the Sm–Nd system and the effects of trace

- mineral inclusions. *Geochimica et Cosmochimica Acta*, **64**, 3413–3432.
- SENGÖR, A.M.C. 1984. *The Cimmeride Orogenic System and the Tectonics of Eurasia*. Geological Society of America, Special Paper, **195**, 1–82.
- SHI, R., YANG, J., XU, Z. & QI, X. 2008. The Bangong Lake ophiolite (NW Tibet) and its bearing on the tectonic evolution of the Bangong–Nujiang suture zone. *Journal of Asian Earth Sciences*, **32**, 438–457.
- SMITH, D.C. 1984. Coesite in clinopyroxene in the Caledonides and its implications for geodynamics. *Nature*, **310**, 641–644.
- SOBOLEV, N.V. & SHATSKY, V.S. 1990. Diamond inclusions in garnets from metamorphic rocks – a new environment for diamond formation. *Nature*, **343**, 742–746.
- SONG, S., ZHANG, L.F., NIU, Y.L., SU, L., SONG, B. & LIU, D. Y. 2006. Evolution from oceanic subduction to continental collision: a case study from the Northern Tibetan Plateau based on geochemical and geochronological data. *Journal of Petrology*, **47**, 435–455.
- SONG, S., NIU, Y.L., SU, L. & XIA, X.H. 2013. Tectonics of the North Qilian orogen, NW China. *Gondwana Research*, **23**, 1378–1401.
- SONG, S., NIU, Y., SU, L., ZHANG, C. & ZHANG, L. 2014. Continental orogenesis from ocean subduction, continent collision/subduction, to orogen collapse, and orogen recycling: the example of the North Qaidam UHPM belt, NW China. *Earth-Science Reviews*, **129**, 59–84.
- SPANDLER, C., HERMANN, J. & RUBATTO, D. 2004. Exsolution of thortveitite, yttrialite, and xenotime during low-temperature recrystallization of zircon from New Caledonia, and their significance for trace element incorporation in zircon. *American Mineralogist*, **89**, 1795–1806.
- ST-ONGE, M.R., RAYNER, N., PALIN, R.M., SEARLE, M.P. & WATERS, D.J. 2013. Integrated pressure–temperature–time constraints for the Tso Moriri dome (Northwest India): implications for the burial and exhumation path of UHP units in the western Himalaya. *Journal of Metamorphic Geology*, **31**, 469–504.
- WEI, C.J. & POWELL, R. 2003. Phase relations in high-pressure metapelites in the system KFMASH ( $K_2O$ – $FeO$ – $MgO$ – $Al_2O_3$ – $SiO_2$ – $H_2O$ ) with application to natural rocks. *Contributions to Mineralogy and Petrology*, **145**, 301–315.
- WEI, C.J. & POWELL, R. 2004. Calculated phase relations in high-pressure metapelites in the system NKFMASH ( $Na_2O$ – $K_2O$ – $FeO$ – $MgO$ – $Al_2O_3$ – $SiO_2$ – $H_2O$ ) with application to natural rocks. *Journal of Petrology*, **44**, 183–202.
- WEI, C.J., SU, X.L., LOU, Y.X. & LI, Y.J. 2009. A new interpretation of the conventional thermobarometry in eclogite: evidence from the calculated PT pseudosections. *Acta Petrologica Sinica*, **25**, 2078–2088 [in Chinese with an English abstract].
- WEI, C.J., QIAN, J.H. & TIAN, Z.L. 2013. Metamorphic evolution of medium-temperature ultra-high pressure (MT–UHP) eclogites from the South Dabie orogen, Central China: an insight from phase equilibria modelling. *Journal of Metamorphic Geology*, **31**, 755–774.
- WELLER, O.M., ST-ONGE, M.R., RAYNER, N., WATERS, D.J., SEARLE, M.P. & PALIN, R.M. 2016. U–Pb zircon geochronology and phase equilibria modelling of a mafic eclogite from the Sumdo complex of south-east Tibet: insights into prograde zircon growth and the assembly of the Tibetan plateau. *Lithos*, **262**, 729–741.
- XU, Q., ZHAO, J., YUAN, X., LIU, H. & PEI, S. 2015. Mapping crustal structure beneath southern Tibet: seismic evidence for continental crustal underthrusting. *Gondwana Research*, **27**, 1487–1493.
- YANG, J.S., XU, Z.Q. ET AL. 2006. A possible new HP/UHP (?) metamorphic belt in China: discovery of eclogite in the Lhasa Terrane, Tibet. *Acta Geologica Sinica*, **80**, 1787–1792 [in Chinese with an English abstract].
- YANG, J.S., XU, Z.Q. ET AL. 2009. Discovery of an eclogite belt in the Lhasa block, Tibet: a new border for Paleo-Tethys? *Journal of Asian Earth Sciences*, **34**, 76–89.
- YANG, X.L., ZHANG, L.F., ZHAO, Z.D. & ZHU, D.C. 2014. Metamorphic evolution of glaucophane eclogite from Sumdo, Lhasa block of Tibetan Plateau: phase equilibria and metamorphic P–T path. *Acta Petrologica Sinica*, **30**, 1505–1519 [in Chinese with an English abstract].
- YIN, A. & HARRISON, T.M. 2000. Geologic evolution of the Himalayan–Tibet orogen. *Annual Review of Earth and Planetary Sciences*, **28**, 211–280.
- ZENG, L.S., LIU, J., GAO, L.E., CHEN, F.Y. & XIE, K.J. 2009. Early Mesozoic high-pressure metamorphism within the Lhasa Block, Tibet and its implications for regional tectonics. *Earth Science Frontiers*, **16**, 140–151 [in Chinese with an English abstract].
- ZHAI, Q.G., ZHANG, R.Y., JAHN, B.M., LI, C., SONG, S.G. & WANG, J. 2011. Triassic eclogites from central Qiangtang, northern Tibet, China: petrology, geochronology and metamorphic P–T path. *Lithos*, **125**, 173–189.
- ZHANG, D.D., ZHANG, L.F. & ZHAO, Z.D. 2011. A study of metamorphism of Sumdo eclogite in Tibet, China. *Earth Science Frontiers*, **18**, 116–126 [in Chinese with an English abstract].
- ZHANG, H.F., XU, W.C., GUO, J.Q., ZONG, K.Q., CAI, H.M. & YUAN, H.L. 2007. Indosinian orogenesis of the Gangdise terrane: evidences from zircon U–Pb dating and petrogenesis of granitoids. *Earth Science*, **32**, 155–166 [in Chinese with an English abstract].
- ZHANG, J., SANTOSH, M., WANG, X., GUO, L., YANG, X. & ZHANG, B. 2012. Tectonics of the northern Himalaya since the India–Asia collision. *Gondwana Research*, **21**, 939–960.
- ZHANG, L.F., ELLIS, D.J., ARCULUS, R.J., JIANG, W. & WEI, C. 2003. ‘Forbidden zone’ subduction of sediments to 150 km depth – the reaction of dolomite to magnesite plus aragonite in the UHPM metapelites from western Tianshan, China. *Journal of Metamorphic Geology*, **21**, 523–529.
- ZHANG, L.F., DU, J.X. ET AL. 2013. A huge oceanic-type UHP metamorphic belt in southwestern Tianshan, China: peak metamorphic age and P–T path. *Chinese Science Bulletin*, **58**, 4378–4383 [in Chinese with an English abstract].
- ZHANG, R.Y., JAHN, B.M. ET AL. 2010. Origin and tectonic implication of an UHP metamorphic mafic–ultramafic complex from the Sulu UHP terrane, eastern China: evidence from petrological and geochemical studies of CCSD–Main Hole core samples. *Chemical Geology*, **276**, 69–87.

- ZHANG, Z.M. & SANTOSH, M. 2012. Tectonic evolution of Tibet and surrounding regions. *Gondwana Research*, **21**, 1–3.
- ZHANG, Z.M., DONG, X., LIU, F., LIN, Y.H., YAN, R. & SANTOSH, M. 2012. Tectonic evolution of the Amdo Terrane, central Tibet: petrochemistry and Zircon U–Pb geochronology. *The Journal of Geology*, **120**, 431–451.
- ZHANG, Z.M., DONG, X., SANTOSH, M. & ZHAO, G.C. 2014. Metamorphism and tectonic evolution of the Lhasa terrane, Central Tibet. *Gondwana Research*, **25**, 170–189.
- ZHAO, J., ZHAO, D., ZHANG, H., LIU, H., HUANG, Y., CHENG, H. & WANG, W. 2014. P-wave tomography and dynamics of the crust and upper mantle beneath western Tibet. *Gondwana Research*, **25**, 1690–1699.
- ZHENG, Y.F. 2012. Metamorphic chemical geodynamics in continental subduction zones. *Chemical Geology*, **328**, 5–48.
- ZHU, D.C., MO, X.X., NIU, Y.L., ZHAO, Z.D., WANG, L.Q., PAN, G.T. & WU, F.Y. 2009. Zircon U–Pb dating and in-situ Hf isotopic analysis of Permian peraluminous granite in the Lhasa terrane, southern Tibet: implications for Permian collisional orogeny and paleogeography. *Tectonophysics*, **469**, 48–60.
- ZHU, D.C., ZHAO, Z.D., NIU, Y.L., DILEK, Y. & MO, X.X. 2011a. Lhasa terrane in southern Tibet came from Australia. *Geology*, **39**, 727–730.
- ZHU, D.C., ZHAO, Z.D. ET AL. 2011b. The Lhasa Terrane: record of a microcontinent and its histories of drift and growth. *Earth and Planetary Science Letters*, **301**, 241–255.
- ZHU, D.C., ZHAO, Z.D. ET AL. 2012. Cambrian bimodal volcanism in the Lhasa Terrane, southern Tibet: record of an early Paleozoic Andean-type magmatic arc in the Australian proto-Tethyan margin. *Chemical Geology*, **328**, 290–308.
- ZHU, D.C., ZHAO, Z.D., NIU, Y.L., DILEK, Y., HOU, Z.Q. & MO, X.X. 2013. The origin and pre-Cenozoic evolution of the Tibetan Plateau. *Gondwana Research*, **23**, 1429–1454.